TITLE:

Extreme deformability of insect cell membranes is governed by phospholipid scrambling

AUTHOR(S):

Shiomi, Akifumi; Nagao, Kohjiro; Yokota, Nobuhiro; Tsuchiya, Masaki; Kato, Utako; Juni, Naoto; Hara, Yuji; ... Yesylevsky, Semen; Bogdanov, Mikhail; Umeda, Masato

CITATION:

Shiomi, Akifumi ...[et al]. Extreme deformability of insect cell membranes is governed by phospholipid scrambling. Cell Reports 2021, 35(10): 109219.

ISSUE DATE:

2021-06

URL:

http://hdl.handle.net/2433/263314

RIGHT:

© 2021 The Author(s).; This is an open access article under the Creative Commons Attribution 4.0 International Public License.

京都大学学術情報リポジトリ
KURENAI 紅
Kyoto University Research Information Repository

京都大学 KYOTO UNIVERSITY
A Self-archived copy in
Kyoto University Research Information Repository
https://repository.kulib.kyoto-u.ac.jp
京都大学学術情報リポジトリ KURENAI 紅 Kyoto University Research Information Repository

Article

Cell Reports

Extreme deformability of insect cell membranes is governed by phospholipid scrambling

Graphical abstract

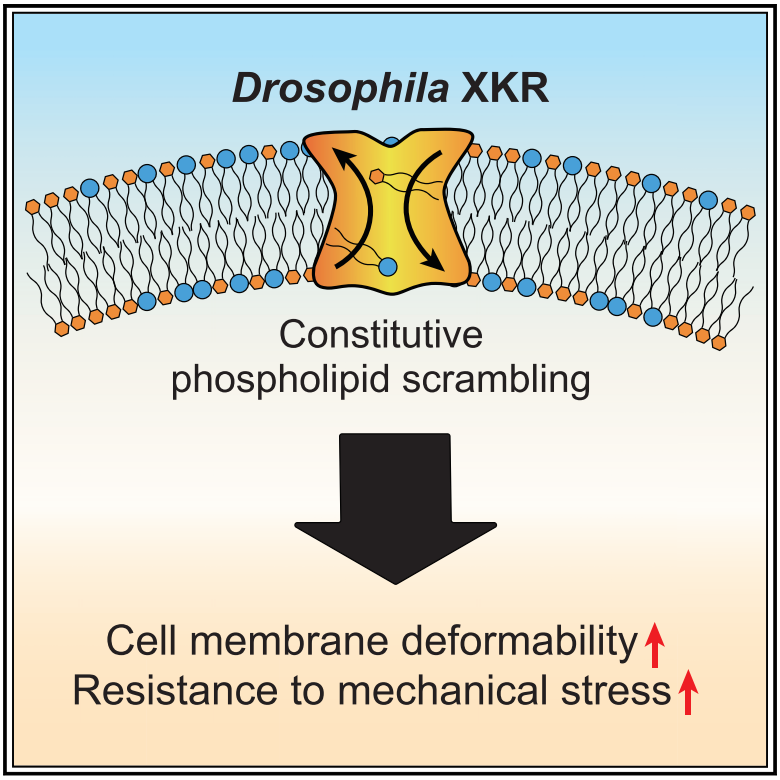

Authors

Akifumi Shiomi, Kohjiro Nagao, Nobuhiro Yokota, ..., Semen Yesylevsky, Mikhail Bogdanov, Masato Umeda

Correspondence

nagao@sbchem.kyoto-u.ac.jp (K.N.),
umeda@sbchem.kyoto-u.ac.jp (M.U.)

In brief

Shiomi et al. show that *Drosophila* cells possess a cell membrane with extreme deformability and resistance to mechanical stress, where constitutively active phospholipid scramblase XKR disturbs the asymmetric distribution of phospholipids and promotes the deformability of cell membranes by regulating both actin cortex dynamics and mechanical properties of the phospholipid bilayer.

Highlights

- Compared with mammalian cells, *Drosophila* cells have a highly elastic cell membrane
- *Drosophila* XKR promotes membrane deformation by constitutive phospholipid scrambling
- Phospholipid scrambling affects actin cortex dynamics and lipid bilayer mechanics
- Deformability of mammalian cells can also be enhanced by phospholipid scrambling

Shiomi et al., 2021, Cell Reports *35*, 109219
June 8, 2021 © 2021 The Author(s).
https://doi.org/10.1016/j.celrep.2021.109219

CellPress

京都大学 KYOTO UNIVERSITY
A Self-archived copy in
Kyoto University Research Information Repository
https://repository.kulib.kyoto-u.ac.jp
京都大学学術情報リポジトリ KURENAI 紅 Kyoto University Research Information Repository

Cell Reports

CellPress OPEN ACCESS

Article

Extreme deformability of insect cell membranes is governed by phospholipid scrambling

Akifumi Shiomi,[1] Kohjiro Nagao,[1,*] Nobuhiro Yokota,[1] Masaki Tsuchiya,[1] Utako Kato,[1] Naoto Juni,[1] Yuji Hara,[1] Masayuki X. Mori,[1] Yasuo Mori,[1] Kumiko Ui-Tei,[2] Motohide Murate,[3] Toshihide Kobayashi,[3] Yuri Nishino,[4] Atsuo Miyazawa,[4] Akihisa Yamamoto,[5] Ryo Suzuki,[5] Stefan Kaufmann,[6] Motomu Tanaka,[5,6] Kazuya Tatsumi,[7] Kazuyoshi Nakabe,[7] Hirofumi Shintaku,[8] Semen Yesylevsky,[9,10] Mikhail Bogdanov,[11] and Masato Umeda[1,12,13,*]

[1]Department of Synthetic Chemistry and Biological Chemistry, Graduate School of Engineering, Kyoto University, Katsura, Kyoto 615-8510, Japan
[2]Department of Biological Sciences, Graduate School of Science, The University of Tokyo, 7-3-1 Hongo, Bunkyo-ku, Tokyo 113-0033, Japan
[3]UMR 7021 CNRS, Faculté de Pharmacie, Université de Strasbourg, 74 Route du Rhin, 67401 Illkirch, France
[4]Graduate School of Life Science, University of Hyogo, Kouto, Kamigori-cho, Ako-gun, Hyogo 678-1297, Japan
[5]Center for Integrative Medicine and Physics, Institute for Advanced Study, Kyoto University, Kyoto 606-8501, Japan
[6]Physical Chemistry of Biosystems, Institute of Physical Chemistry, University of Heidelberg, 69120 Heidelberg, Germany
[7]Department of Mechanical Engineering and Science, Kyoto University, Katsura, Kyoto 615-8540, Japan
[8]Microfluidics RIKEN Hakubi Research Team, RIKEN Cluster for Pioneering Research, Wako, Saitama 351-0198, Japan
[9]Laboratoire Chrono Environnement UMR CNRS 6249, Université de Bourgogne Franche-Comté, 16 Route de Gray, 25030 Besançon Cedex, France
[10]Department of Physics of Biological Systems, Institute of Physics of the National Academy of Sciences of Ukraine, Prospect Nauky 46, 03680 Kyiv, Ukraine
[11]Department of Biochemistry & Molecular Biology, University of Texas Health Science Center at Houston, McGovern Medical School, 6431 Fannin, Houston, TX 77030, USA
[12]Present address: HOLO BIO Co., Ltd, Katsura Innovation Park 1-36, Nishikyo-ku, Kyoto 615-8245, Japan
[13]Lead contact
*Correspondence: nagao@sbchem.kyoto-u.ac.jp (K.N.), umeda@sbchem.kyoto-u.ac.jp (M.U.)
https://doi.org/10.1016/j.celrep.2021.109219

SUMMARY

Organization of dynamic cellular structure is crucial for a variety of cellular functions. In this study, we report that *Drosophila* and *Aedes* have highly elastic cell membranes with extremely low membrane tension and high resistance to mechanical stress. In contrast to other eukaryotic cells, phospholipids are symmetrically distributed between the bilayer leaflets of the insect plasma membrane, where phospholipid scramblase (XKR) that disrupts the lipid asymmetry is constitutively active. We also demonstrate that XKR-facilitated phospholipid scrambling promotes the deformability of cell membranes by regulating both actin cortex dynamics and mechanical properties of the phospholipid bilayer. Moreover, XKR-mediated construction of elastic cell membranes is essential for hemocyte circulation in the *Drosophila* cardiovascular system. Deformation of mammalian cells is also enhanced by the expression of *Aedes* XKR, and thus phospholipid scrambling may contribute to formation of highly deformable cell membranes in a variety of living eukaryotic cells.

INTRODUCTION

Cell structure is dynamic and flexible, which allows a broad range of cellular functions (McMahon and Gallop, 2005). The dynamic cellular structures are cooperatively organized by multiple cellular components, including the plasma membrane, cytoskeleton, cytoplasm, and nucleus. Among them, the plasma membrane is particularly important for determining cell shape and confers cells with mechanical robustness against extrinsic mechanical stresses (Diz-Muñoz et al., 2013; Janmey and Kinnunen, 2006). The structure and mechanical properties of the plasma membrane are mainly determined by the actin cortex, a cytoskeleton spreading over the inner surface of plasma membranes (Gauthier et al., 2012; Sheetz, 2001). The architecture of the actin cortex can be actively regulated by the dynamic organization and remodeling of its components, including actin filaments, linker proteins, and myosin motors (Chugh et al., 2017; Tan et al., 2008). Moreover, the phospholipid bilayer also regulates the structure and mechanical properties of the plasma membrane. Actin cortex-associated proteins, such as moesin, talin, and N-WASP, have been shown to bind to specific phospholipids of the plasma membrane, which provides the mechanisms by which the actin cortex architecture is regulated (Charras et al., 2006; Fritzsche et al., 2014). The plasma membrane's phospholipid composition and sterol content directly influence the physicochemical properties of phospholipid bilayers themselves (Evans and Needham, 1987). Since each leaflet of the bilayer membrane exhibits distinct lipid and protein compositions, it has been proposed that the phospholipid distribution between leaflets also determines the mechanical properties of

This is an open access article under the CC BY license (http://creativecommons.org/licenses/by/4.0/).

京都大学 KYOTO UNIVERSITY
A Self-archived copy in
Kyoto University Research Information Repository
https://repository.kulib.kyoto-u.ac.jp
京都大学学術情報リポジトリ KURENAI 紅 Kyoto University Research Information Repository

plasma membrane (Sheetz et al., 1976; Sheetz and Singer, 1974). However, how these regulatory mechanisms could be integrated to organize the dynamic structure of cell membranes has remained unclear.

In plasma membranes of eukaryotes, phosphatidylethanolamine (PE) and phosphatidylserine (PS) are present in the inner leaflet of the bilayer membrane, whereas phosphatidylcholine (PC) molecules are mainly present in its outer leaflet (Murate et al., 2015; van Meer et al., 2008). The distribution of phospholipids across the plasma membrane bilayer is actively regulated by a class of membrane-bound proteins known as phospholipid translocators (Pomorski and Menon, 2016). The phospholipid flippase complex, formed by type 4 subfamily P-type adenosine triphosphatases (P4-ATPases) and CDC50 family proteins, plays a dominant role in maintaining the asymmetrical distribution of membrane phospholipids (Sebastian et al., 2012). This is achieved by transporting PE and PS from the outer leaflet to the inner leaflet of the plasma membrane (Panatala et al., 2015; Tsuchiya et al., 2018). In mammalian cells, this asymmetrical distribution of phospholipids is disrupted by the action of phospholipid scramblases, such as transmembrane protein 16F (TMEM16F) and XK-related protein 8 (Xkr8) (Suzuki et al., 2010, 2013). TMEM16F is responsible for exposing PS on the cell surface of activated platelets (Suzuki et al., 2010). The mammalian scramblase Xkr8 is activated by cleavage of its C-terminal domain by caspases during apoptosis, thereby causing phospholipid scrambling and PS exposure on the cell surface, which serves as an "eat me" signal (Suzuki et al., 2013). A recent study by Sakuragi et al. (2019) demonstrated that Xkr8's scrambling activity can be stimulated by kinase-mediated phosphorylation, independent of caspase-mediated cleavage, but the physiological function of phospholipid scrambling in non-apoptotic cells remains to be elucidated.

Insects are the most diversified group of animal on Earth (Scheffers et al., 2012). During the course of evolution, some insects successfully achieved extreme miniaturization of their body sizes (Hanken and Wake, 1993). Insects with a body size of several millimeters, such as flies, and even the smallest insects with a body size comparable to that of unicellular organisms, such as *Megaphragma mymaripenne*, possess highly developed nervous, circulatory, and respiratory systems (Polilov, 2015). Such miniaturization has been achieved not only by restructuring the architecture of organ systems, but also by decreasing the size of organ systems while retaining their structural and functional features (Hanken and Wake, 1993; Polilov, 2015). Flies are one of the most agile flying animals that exhibit vigorous movements of organ systems, such as the muscular and cardiovascular systems (Kammer and Heinrich, 1978). The reduced body size together with the need for agile movements imposes steep mechanical constraints on the dynamic structures of cellular systems that construct miniaturized organ systems; however, the cellular and molecular bases underlying this remain unclear.

In this study, we revealed that *Drosophila* cells have highly deformable cell membranes, with extremely low membrane tension and high resistance to mechanical stress. We also found that phospholipids are symmetrically distributed between the outer and inner leaflets of *Drosophila* plasma membrane, in which the constitutively active phospholipid scramblase XKR bi-directionally transports phospholipids between the leaflets. Our findings also showed that *Drosophila* XKR is a crucial determinant of elastic properties of cell membranes by regulating both the actin cortex dynamics and the mechanical properties of the phospholipid bilayer. We discuss implications of our results for the mechanism underlying the formation of highly deformable cell membranes using constitutively active phospholipid scramblase.

RESULTS

Extreme deformability and high resistance to mechanical stress of *Drosophila* cells

During the course of studying the biological functions of cell membranes (Murakami et al., 2017; Shiomi et al., 2020; Tsuchiya et al., 2018), we found that *Drosophila* cells were easily aspirated into capillary vessels with inner diameters of <1 μm (Figure 1A; Video S1). *Drosophila* cell lines derived from embryos (Kc167 and S2 cells) and the central nervous system (BG2-c2, BG2-c6, and BG3-c2 cells) could be aspirated at −50 mmHg of suction within 30 s, corresponding to the aspiration of 20%−40% of the total cell volume (Figure 1B). Under the same experimental conditions, an *Aedes* cell line (C6/36) was also aspirated into the capillary vessel. Such extreme deformability was not observed with mammalian (THP-1, CHO-K1, Eph4, HeLa, and PC3) or moth (Sf9) cell lines; none of these cells was aspirated into the capillary vessel under the same experimental conditions, and higher pressure aspiration resulted in the plasma membrane being torn off.

To quantitatively evaluate membrane deformability on the whole-cell scale, we used a micropipette aspiration assay to determine the membrane tension and Young's modulus of the plasma membrane (Figure 1C) (Hochmuth, 2000). The *Drosophila* and *Aedes* cell lines had remarkably low membrane tensions (range, 18.5 ± 7.0 to 27.8 ± 16.4 pN/μm) and Young's moduli (range, 16.9 ± 6.4 to 21.9 ± 7.0 Pa) compared with those obtained for the mammalian cell lines in the present study (Figures 1D, 1E, and S1A–S1C) and those reported in previous studies (Jones et al., 1999; Rodriguez et al., 2013; Shiomi et al., 2020). In addition, we used a microflow device to examine the survival of cells after consecutive exposures to fluid shear stress produced by passage through a needle (Figure 1F) (Barnes et al., 2012). A significant proportion of the mammalian cells was disrupted upon exposure to extensive fluid shear stress (640 Pa/cm^2), as previously reported (Barnes et al., 2012), whereas *Drosophila* cells (Kc167, S2, and BG2-c6) were highly resistant to even repeated exposure to extensive fluid shear stress (Figure 1G). These results showed that *Drosophila* cells possess a cell membrane with extreme deformability and resistance to mechanical stresses.

Symmetrical distribution of phospholipids in the plasma membrane of *Drosophila* cells

In *Drosophila* (Kc167, S2, BG2-c2, BG2-c6, and BG3-c2) and *Aedes* (C6/36) cell lines, PE, a cone-shaped lipid that tends to form a non-bilayer structure, comprises >40% of the total phospholipids and 65% of those in the plasma membrane of the

京都大学 KYOTO UNIVERSITY
A Self-archived copy in
Kyoto University Research Information Repository
https://repository.kulib.kyoto-u.ac.jp
京都大学学術情報リポジトリ KURENAI 紅 Kyoto University Research Information Repository

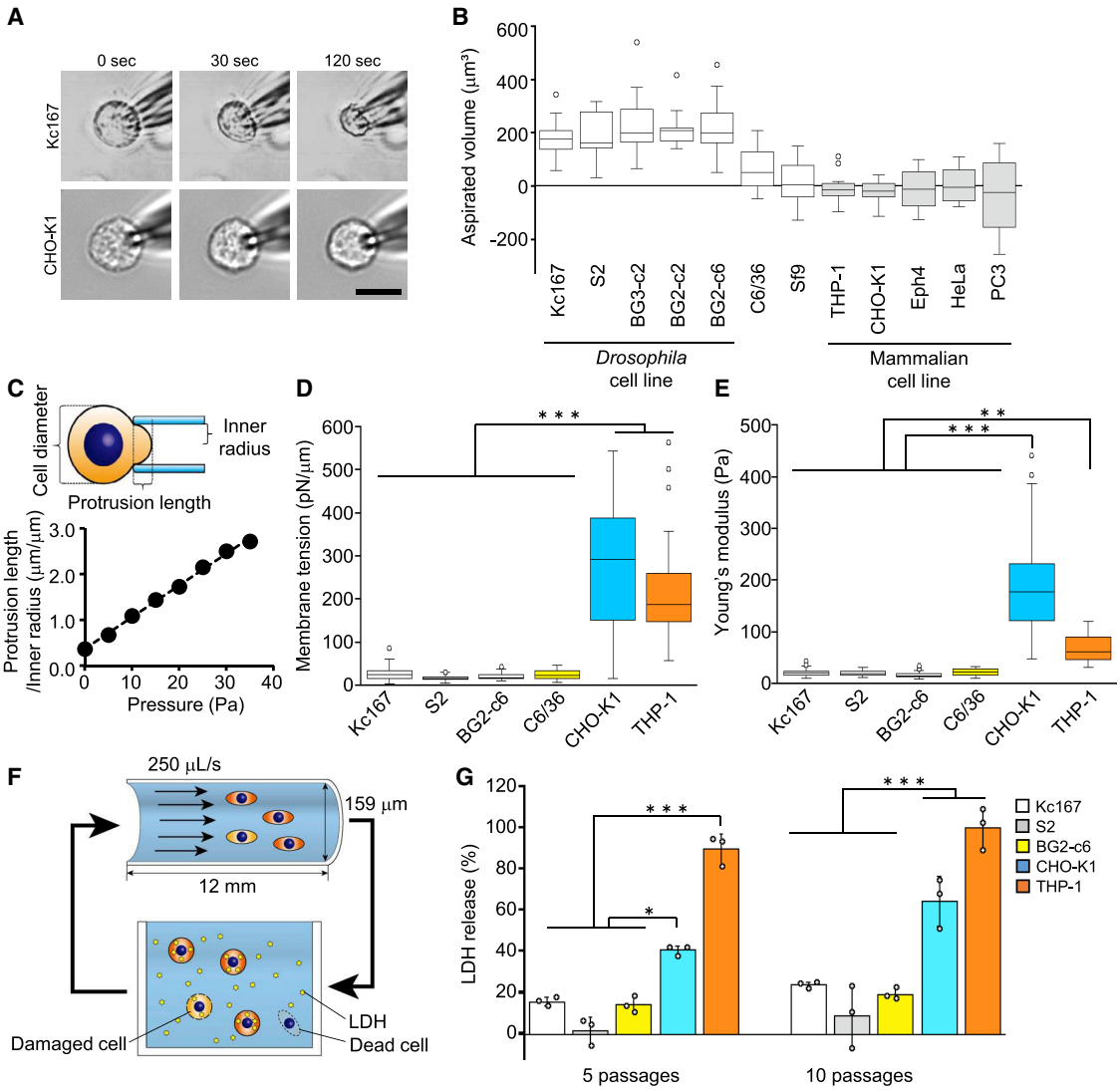

Figure 1. Extreme deformability and high resistance to mechanical stress of *Drosophila* cells

(A) Kc167 and CHO-K1 cells were aspirated into capillary vessels at −50 mmHg for 0, 30, and 120 s. Scale bar, 10 μm.

(B) Cellular volumes aspirated at −50 mmHg for 30 s for Kc167 (n = 24), S2 (n = 10), BG3-c2 (n = 10), BG2-c2 (n = 10), BG2-c6 (n = 22), C6/36 (n = 22), Sf9 (n = 10), THP-1 (n = 11), CHO-K1 (n = 10), Eph4 (n = 11), HeLa (n = 10), and PC3 (n = 10) cells.

(C) (Top) Schematic of the micropipette aspiration assay. (Bottom) Representative data from the micropipette aspiration assay for Kc167 cells. Membrane tension and Young's modulus were calculated from the linear function using the law of Laplace and the theoretical model.

(D and E) Membrane tensions and Young's moduli of Kc167 (n = 19), S2 (n = 23), BG2-c6 (n = 23), C6/36 (n = 20), CHO-K1 (n = 22), and THP-1 (n = 31) cells.

(F and G) Cells were passed through a narrow capillary (159-μm inner diameter, 12-mm length) at a constant flow rate (250 μL/s) 5 or 10 times. (G) Leakage of intracellular lactate dehydrogenase (LDH) into medium was analyzed.

For boxplots, center mark is median, whiskers are minimum/maximum excluding outliers, and circles are outliers (B, D, and E). Mean ± SD (G). Tukey's test (D, E, and G). *p < 0.05, **p < 0.01, ***p < 0.001.

Kc167 cell line (Table S1; Figures S2A and S2B). In contrast, PC, a typical bilayer-forming lipid, contributes >55% of membrane phospholipids in mammalian cells examined in this study (Table S1) as well as in other eukaryotic cells (Vance, 2015).

In many eukaryotic plasma membranes, amino phospholipids such as PE and PS reside in the inner leaflet of the bilayer membrane (Murate et al., 2015; van Meer et al., 2008). This asymmetrical distribution of phospholipids produces differences in the lipid composition and the electrostatic properties of each leaflet of bilayer membrane, which in turn influences the actin cortex dynamics that are intimately linked to the mechanical properties of cell membranes (Diz-Muñoz et al., 2013; Sheetz et al., 2006; Tsuchiya et al., 2018). Consistent with previous reports (Emoto et al., 1996), binding of a PE-specific probe (fluorescein isothiocyanate-conjugated streptavidin and biotinylated Ro09-0198 [FITC-SA-Ro]) and PS-specific probe (EGFP-annexin V) to cell

京都大学 KYOTO UNIVERSITY
A Self-archived copy in
Kyoto University Research Information Repository
https://repository.kulib.kyoto-u.ac.jp
京都大学学術情報リポジトリ KURENAI 紅 Kyoto University Research Information Repository

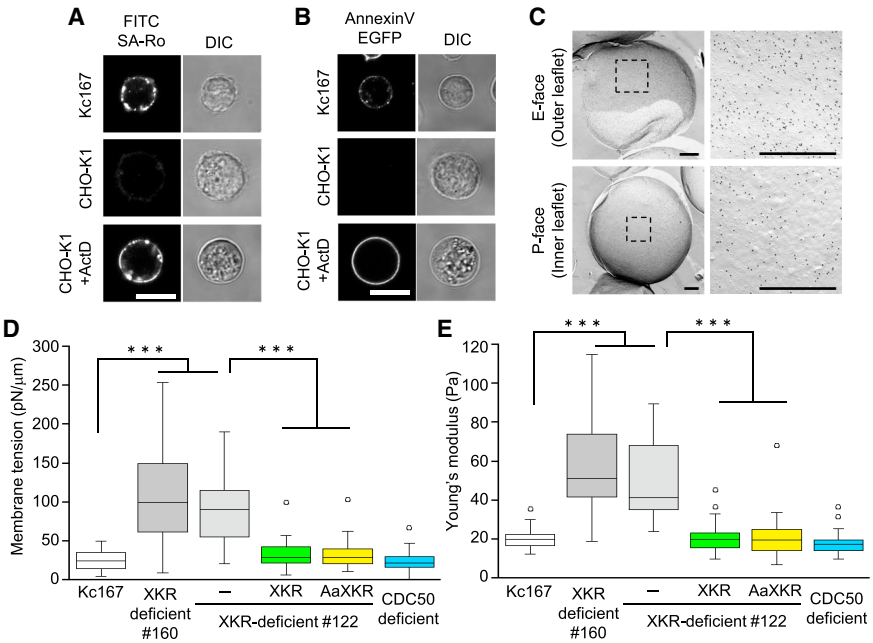

Figure 2. Phospholipid scramblase XKR facilitates deformability of cell membranes

(A and B) Binding of FITC-SA-Ro and annexin V-EGFP to the cell surface of Kc167 and CHO-K1 cells treated with or without actinomycin D (ActD). DIC, differential interference contrast. Scale bars, 10 μm.

(C) Binding of biotinylated duramycin to the E-face (outer leaflet) or P-face (inner leaflet) of the plasma membranes of Kc167 cells. Bound biotinylated duramycin was labeled with gold-conjugated anti-biotin antibody. Right panels are enlargement of the boxed area of left panels. Scale bars, 1 μm.

(D and E) Membrane tensions and Young's moduli of Kc167 (n = 23), XKR-deficient #160 (n = 20), XKR-deficient #122 (n = 41), EGFP-XKR-expressing XKR-deficient #122 (n = 42), EGFP-AaXKR-expressing XKR-deficient #122 (n = 25), and CDC50-deficient cells (n = 42).

For boxplots, center mark is median, whiskers are minimum/maximum excluding outliers, and circles are outliers (D and E). Tukey's test (D and E). ***$p < 0.001$.

surfaces was observed in mammalian CHO-K1 cells only when the asymmetrical distribution of phospholipids was disrupted by inducing apoptosis using actinomycin D (ActD) (Figures 2A and 2B). However, unexpectedly, we observed intense binding of FITC-SA-Ro as well as EGFP-annexin V to the cell surface of living Kc167 cells. Thus, PE and PS are located in the outer leaflet of plasma membrane in *Drosophila* cells, which contrasts to the case in mammalian cells where they are exclusively localized in the inner leaflet.

The trans-bilayer distribution of phospholipids was further evaluated using the sodium dodecyl sulfate-digested freeze-fracture replica labeling (SDS-FRL) technique, in which binding of lipid-specific probes to either the outer or inner leaflet monolayers of SDS-treated, freeze-fractured membranes is detected using colloidal gold-conjugated secondary antibodies (Murate et al., 2015). In Kc167 cells, gold particles bound to PE were found in both the outer leaflet (E-face) and the inner leaflet (P-face) of the plasma membrane (Figure 2C). The average number of gold particles/μm^2 was 93.3 ± 34.9 (n = 22, mean ± SD) on the E-face and 55.5 ± 26.5 (n = 24, mean ± SD) on the P-face, indicating the presence of 62.7% of PE molecules in the outer leaflet of the plasma membrane. Moreover, SDS-FRL analysis using a PS- and phosphatidylinositol (PI)-binding probe also showed that 40.6% of the bound probe was present on the outer leaflet of the plasma membrane (Figure S2C). These results clearly demonstrate that the asymmetrical trans-bilayer distribution of phospholipids is lost in the plasma membrane of *Drosophila* cells.

Identification of the phospholipid scramblase XKR as a crucial regulator of the elastic deformation of *Drosophila* cell membranes

Because the *Drosophila* plasma membrane exhibits features of high deformability and the symmetric distribution of phospholipids, we investigated any potential inter-relationship between these two features. To examine whether the trans-bilayer relocation of phospholipid molecules is responsible for the enhanced deformability of *Drosophila* cell membranes, we focused on lipid transporters including phospholipid flippases (P4-ATPases [CG4301, CG9981, CG14741, CG31729, CG33298, and CG42321], CDC50 family [CG9947]) and phospholipid scramblases (XKR family [CG32579], TMEM16 family [CG6938]) and suppressed their expression in Kc167 cells, followed by an evaluation of the mechanical properties of the plasma membrane. Among them, we found that the suppressing XKR (CG32579), a *Drosophila* homolog of Xkr8, caused remarkable changes in deformability (Figures S3A and S3B).

For precise evaluation of XKR's contribution to cell deformation, we established mutant cell lines using CRISPR-Cas9 (Figures S3C–S3E). In the XKR-deficient mutant cells (#122), the membrane tension and Young's modulus were increased by 4.1-fold and 2.7-fold, respectively, compared with the levels in control cells (Figures 2D, 2E, and S1D). This decrease in deformability was also observed in independent XKR-deficient mutant cell line (#160) and completely rescued by the re-expression of XKR. In contrast, deficiency in *Cdc50*, a *Drosophila* gene encoding a CDC50 family protein required for P4-ATPase (main subunit of phospholipid flippase) translocation to the plasma membrane, did not significantly affect Kc167 membrane deformability. As there were no obvious structural changes in the plasma membrane of XKR-deficient cells under an electron microscope (Figure S4A), the effects of XKR depletion on the mechanical properties of cell membranes were not due to disruption of the membrane bilayer structure. These findings clearly show that XKR plays a crucial role in the formation of *Drosophila* cell membranes with extreme deformability.

京都大学 KYOTO UNIVERSITY
A Self-archived copy in
Kyoto University Research Information Repository
https://repository.kulib.kyoto-u.ac.jp
京都大学学術情報リポジトリ KURENAI 紅 Kyoto University Research Information Repository

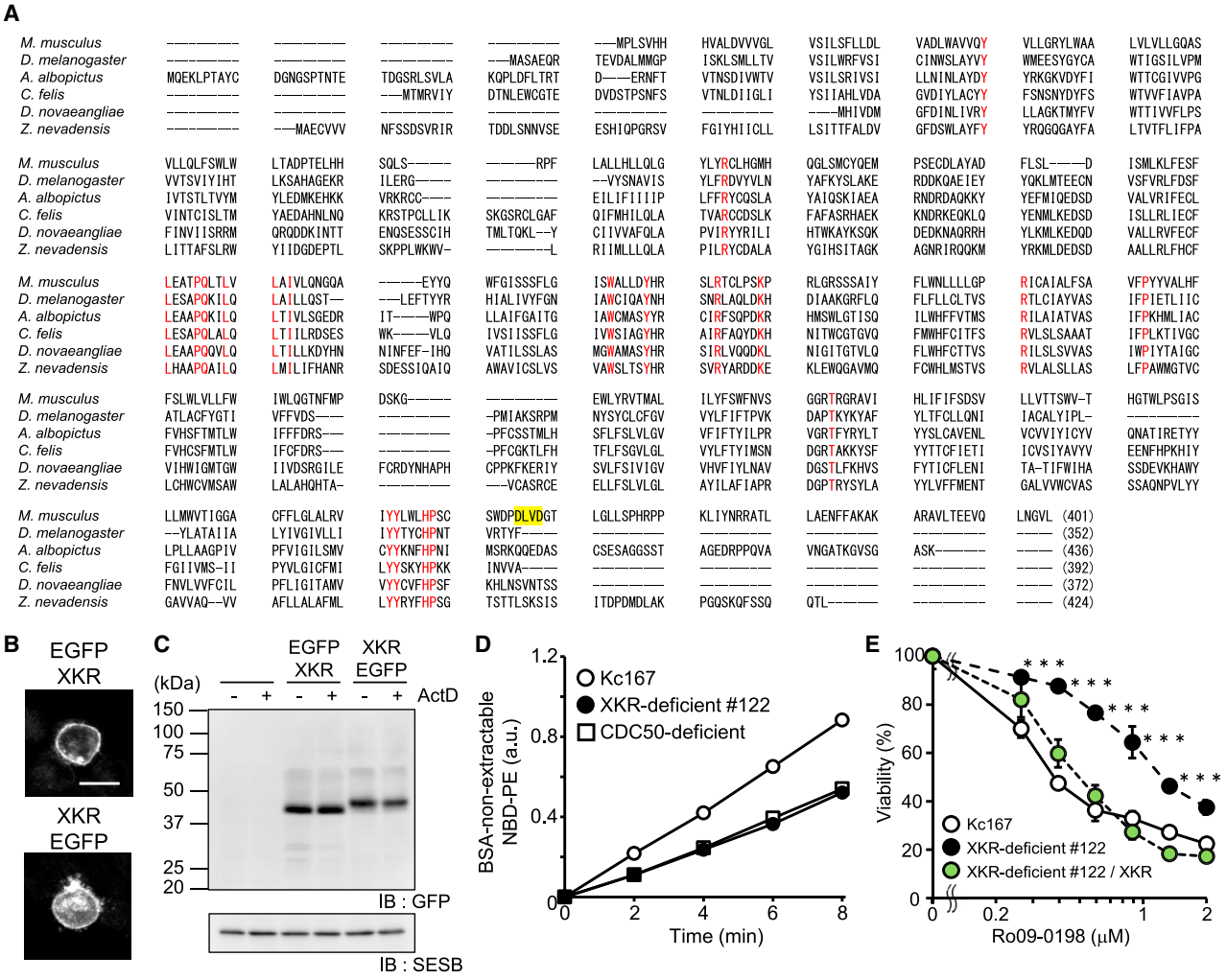

Figure 3. XKR-facilitated constitutive phospholipid scrambling in living cells

(A) The amino acid sequences of mouse Xkr8 and five insect XKR proteins were compared, including *Mus musculus* (NP_958756.1), *Drosophila melanogaster* (NP_727957.1), *Aedes albopictus* (XP_019533658.1), *Ctenocephalides felis* (XP_026467720.1), *Dufourea novaeangliae* (KZC09005.1), and *Zootermopsis nevadensis* (XP_021921864.1). The caspase recognition site (DxxD motif) is highlighted in yellow. Conserved residues are shown in red.

(B) Localization of EGFP-XKR and XKR-EGFP in Kc167 cells. Scale bar, 10 μm.

(C) Kc167 cells expressing EGFP-XKR or XXR-EGFP were incubated with ActD for 6 h, and cell lysates were analyzed by immunoblotting with anti-GFP or anti-SESB antibodies. The amount of SESB was analyzed as a loading control.

(D) Kc167, XKR-deficient #122, and CDC50-deficient cells were incubated with 0.4 μM NBD-PE at 15°C for 0, 2, 4, 6, and 8 min. After washing with bovine serum albumin (BSA), fluorescence intensity was determined by fluorescence-activated cell sorting. The mean fluorescence intensity of 10,000 cells at each incubation time is plotted.

(E) Kc167, XKR-deficient #122, and XKR re-expressed cells were incubated with Ro09-0198 in Schneider's *Drosophila* medium at 25°C for 1 h. Cellular viability was analyzed by an MTS (3-(4,5-dimethylthiazol-2-yl)-5-(3-carboxymethoxyphenyl)-2-(4-sulfophenyl)-2*H*-tetrazolium) assay (n = 3).

Mean ± SD (E). Tukey's test (E). ***p < 0.001.

Drosophila XKR facilitates constitutive scrambling of phospholipids in living cells

The mammalian scramblase Xkr8 is activated by cleavage of its C-terminal domain by caspases during apoptosis, leading to phospholipid scrambling and the exposure of PS on the cell surface (Suzuki et al., 2013). We found that *Drosophila* XKR lacks a caspase recognition motif in both of its N- and C-terminal domains (Figure 3A). Since the deformation of living Kc167 cells was shown to be regulated by XKR (Figures 2D and 2E), we hypothesized that XKR is constitutively active and mediates phospholipid scrambling at the plasma membrane in living cells. EGFP-fused XKR localized to the plasma membrane is not cleaved upon caspase activation, as anticipated from the amino acid sequence (Figures 3B, 3C, S4B, and S4C). The inward trans-bilayer movement (from the outer to the inner leaflet of the plasma membrane) of the fluorescent-labeled phospholipid analogs NBD-PE, NBD-PS, and NBD-PC was significantly suppressed in XKR-deficient cells (Figures 3D, S4I, and S4J). In

京都大学 KYOTO UNIVERSITY
A Self-archived copy in
Kyoto University Research Information Repository
https://repository.kulib.kyoto-u.ac.jp
京都大学学術情報リポジトリ KURENAI 紅 Kyoto University Research Information Repository

addition, the cell surface exposure of PE, which was estimated by sensitivity to a PE-binding toxin (Ro09-0198) (Kato et al., 2013), was significantly decreased in XKR-deficient cells compared to control cells and was restored in mutant cells that re-express XKR (Figure 3E). Amounts of PE and PS in the outer leaflet, assessed by cell surface binding of fluorescent-labeled SA-Ro and annexin V, also decreased in XKR-deficient cells (Figures S4E–S4G). In CDC50-deficient cells, the decreased inward trans-bilayer movement of NBD-PE, NBD-PS, and NBD-PC (Figures 3D, S4I, and S4J) and the increased cell surface exposure of PE and PS (Figures S4D–S4F) were observed, indicating that phospholipid flippase also works in Kc167 cells. Thus, in *Drosophila* cells, XKR facilitates constitutive scrambling of phospholipid in the plasma membrane and disturbs the phospholipid flippases-mediated formation of an asymmetric distribution of phospholipid.

XKR confers high deformability to cell membranes by regulating actin cortex dynamics

The mechanical properties of the plasma membrane are mainly regulated by the actin cortex (Chugh et al., 2017). We first measured the thickness of the actin cortex by confocal microscopy imaging of the plasma membrane and cortex (Clark et al., 2013). As shown in Figure 4A, the actin cortex thickness of Kc167 cells was decreased 29% by the depletion of XKR, indicating that XKR regulates the architecture of the actin cortex. To identify the effector proteins involved in the XKR-mediated regulation of the architecture of the actin cortex, we expressed several actin cortex modulators as EGFP-fused proteins and observed their localization intracellularly during the deformation of cells. Although the functions of actin cortex modulators such as myosin and filamin are reportedly regulated by their intracellular distribution (Luo et al., 2013; Salbreux et al., 2012), no apparent differences in the intracellular localization of these proteins were observed between Kc167 and XKR-deficient cells (Figures S5A–S5H). However, the proportion of cells exhibiting abnormal mitosis characterized by bi-nucleation was significantly increased by the expression of moesin (Moe) in XKR-deficient cells, but not in Kc167 cells (Figures S5J). Moe, the sole ERM (ezrin, radixin, and Moe) protein in *Drosophila*, is a linker protein that enhances the mechanical properties of plasma membrane by connecting the phospholipid bilayer and the actin cortex. Moe's function is positively regulated by the phosphorylation of a threonine residue near the C-terminal domain (Fehon et al., 2010). Aberrant accumulation of phosphorylated Moe at polar cortex during cell division induces bi-nucleation (Roubinet et al., 2011). In addition, studies have shown that Moe controls cellular stiffness by regulating actin dynamics in *Drosophila* S2 cells (Kunda et al., 2008). Thus, we hypothesized that XKR regulates the mechanical properties of the plasma membrane via controlling Moe function.

We analyzed the effects of overexpression of wild-type Moe, non-phosphorylatable Moe mutant (MoeTA), and phosphomimetic Moe mutant (MoeTD) on the mechanical properties of the plasma membrane in Kc167 and XKR-deficient cells (Figures 4B and 4C). Expression levels of wild-type Moe, MoeTA, and MoeTD were comparable in Kc167 and XKR-deficient cells (Figure S5K). The membrane tension and Young's modulus of Kc167 cells were significantly increased by expression of the MoeTD mutant, but they remained unchanged after expression of wild-type Moe, indicating that sufficient endogenous Moe protein for the regulation of cortical actin stiffness is present in Kc167 cells, and that the actin cortex of Kc167 cells may be stiffened by phosphorylated Moe. However, the mechanical properties of Kc167 cells were not changed by expression of the MoeTA mutant, indicating that the cell membrane is not stiffened by endogenously expressed Moe via its phosphorylation in Kc167 cells.

In contrast to Kc167 cells, the membrane tension and Young's modulus of XKR-deficient cells were not increased by expression of the MoeTD mutant, but were significantly decreased by expression of the MoeTA mutant. Because overexpression of wild-type Moe did not affect the membrane tension and Young's modulus in XKR-deficient cells, Moe-induced bi-nucleation is not directly caused by altered cortical actin stiffness. These results suggest that the phosphorylation of Moe is enhanced in XKR-deficient cells, which causes the stiffening of the actin cortex. However, compared with Kc167 cells, the increase in the level of Moe phosphorylation was not observed in XKR-deficient cells (Figure 4D). Moreover, even under conditions of MoeTD overexpression, the membrane tension and Young's modulus of XKR-deficient cells were higher than those in Kc167 cells. Thus, it is likely that XKR regulates the function of Moe in a manner independent of the control of Moe phosphorylation.

Given that the interaction between phosphorylated Moe and the phospholipid bilayer is crucial for the Moe-mediated stiffening of the actin cortex (Coscoy et al., 2002; Fritzsche et al., 2014; Roch et al., 2010), we analyzed the dynamics of Moe proteins on the plasma membrane by a fluorescence recovery after photobleaching (FRAP) assay. The proportion of MoeTD in the mobile (exchangeable) fraction was decreased by the depletion of XKR (Figures 4E and 4F). Furthermore, the proportion of MoeTD localized at the plasma membrane was increased by the depletion of XKR (Figure 4G), indicating that XKR enhances the turnover of phosphorylated Moe. To directly evaluate the contribution of XKR to the regulation of Moe interaction with the phospholipid bilayer, we focused on the FERM domain, which is a lipid-binding domain of Moe and is exposed to the protein surface by its phosphorylation. We expressed the truncated form of the FERM domain and evaluated its turnover on the plasma membrane by a FRAP assay. The proportion of FERM domain in the mobile fraction on the plasma membrane was significantly decreased by the depletion of XKR (Figures 4H and 4I). These results revealed that XKR accelerates the dynamic interaction between Moe and the phospholipid bilayer, which suppresses Moe-mediated stiffening of the actin cortex and contributes to the construction of a highly deformable cell membrane (Figure 4J).

Effect of symmetric trans-bilayer distribution of phospholipids on deformation of the phospholipid bilayer

Given that it has been proposed that the phospholipid bilayer itself is important for determining the mechanical properties of cell membranes (Steinkühler et al., 2019), we hypothesized that XKR also regulates the mechanical properties of the

京都大学 KYOTO UNIVERSITY
A Self-archived copy in
Kyoto University Research Information Repository
https://repository.kulib.kyoto-u.ac.jp
京都大学学術情報リポジトリ KURENAI 紅 Kyoto University Research Information Repository

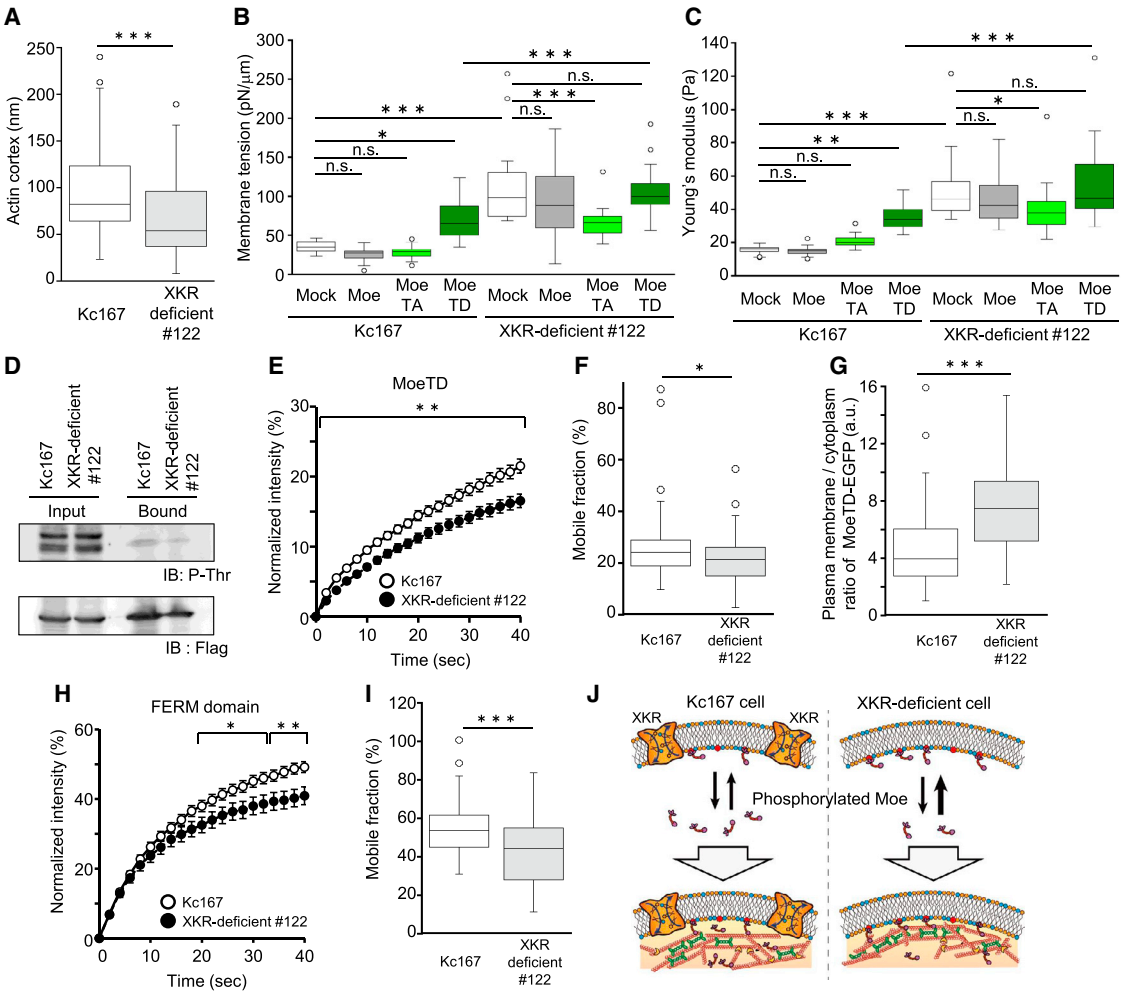

Figure 4. XKR regulates actin cortex architecture by accelerating dynamic interaction between Moe and phospholipid bilayer

(A) Actin cortex thickness in Kc167 (n = 38) and XKR-deficient (n = 37) cells.

(B and C) Membrane tensions and Young's moduli of Kc167 cells expressing mock (n = 13), Moe-EGFP (n = 20), MoeTA-EGFP (n = 21), or MoeTD-EGFP (n = 21), and XKR-deficient cells expressing mock (n = 13), Moe-EGFP (n = 20), MoeTA-EGFP (n = 21), or MoeTD-EGFP (n = 23).

(D) Moe-FLAG proteins were precipitated from cell lysates by anti-FLAG M2 affinity agarose gel. Cell lysate (Input) and precipitated proteins (Bound) were analyzed by immunoblotting with anti-phosphorylated threonine (P-Thr) or anti-FLAG antibodies.

(E and F) Normalized fluorescence recovery (E) and proportions of mobile fraction (F) in MoeTD-EGFP on the plasma membrane of Kc167 (n = 54) and XKR-deficient cells (n = 58).

(G) Distribution of MoeTD-EGFP to plasma membrane of Kc167 (n = 58) and XKR-deficient #122 cells (n = 48).

(H and I) Normalized fluorescence recovery (H) and proportions of mobile fraction (I) in EGFP-fused FERM domain on the plasma membrane of Kc167 (n = 55) and XKR-deficient cells (n = 55).

(J) Model for the XKR-mediated regulation of actin cytoskeleton. XKR accelerates the dynamic interaction between Moe and the plasma membrane, which suppresses Moe-mediated stiffening of actin cortex.

For boxplots, center mark is median, whiskers are minimum/maximum excluding outliers, and circles are outliers (A–C, F, G, and I). Mean ± SEM (E and H). Student's t test (A and E–I). Tukey's t test (B and C). *p < 0.05, **p < 0.01, ***p < 0.001; n.s., not significant.

phospholipid bilayer via regulating the trans-bilayer distribution of phospholipids. First, we investigated the effect of the trans-bilayer distribution of phospholipids on the phospholipid bilayer deformation by coarse-grained molecular dynamics simulations (Marrink et al., 2007). Membrane extrusion through a pore of 30 nm in diameter was simulated by pumping water with a mechanical piston moving at a constant velocity on a timescale of hundreds of nanoseconds (Figure 5A; Video S2). In these simulations, the elastic rigidity of the membrane was proportional to the mean reaction force acting on the piston. Three piston velocities were compared for symmetrical and asymmetrical phospholipid bilayers with compositions resembling those of *Drosophila* cells (Figure S6A). The asymmetrical membrane was shown to be 1.3- to 3.4-fold more rigid than the symmetrical membrane, depending on the speed of deformation (Figures 5B–5E). This suggests that the symmetrical distribution

京都大学 KYOTO UNIVERSITY
A Self-archived copy in
Kyoto University Research Information Repository
https://repository.kulib.kyoto-u.ac.jp
京都大学学術情報リポジトリ KURENAI 紅 Kyoto University Research Information Repository

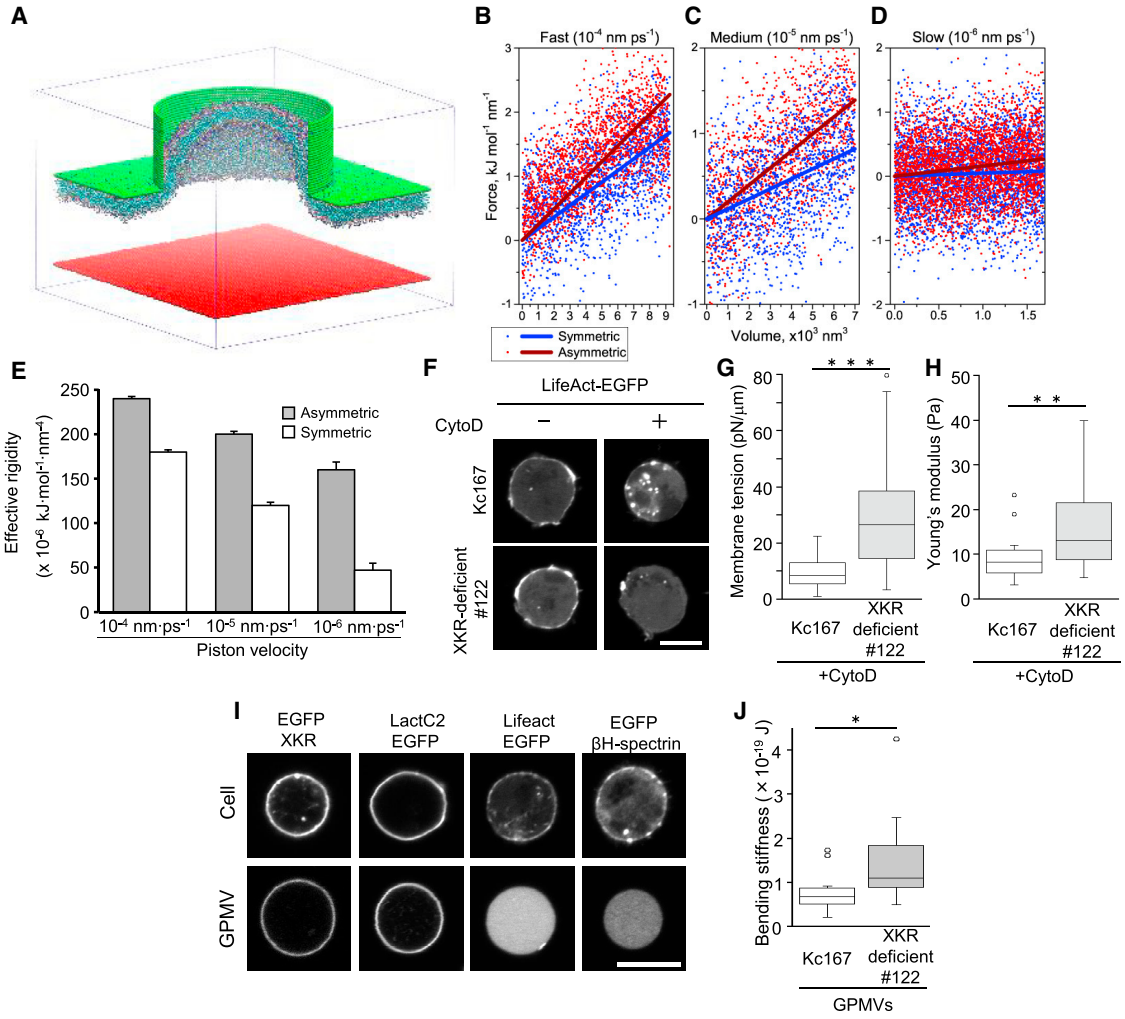

Figure 5. XKR regulates the mechanical properties of the phospholipid bilayer

(A) Schematic of the molecular dynamics simulations of membrane protrusion. The piston particles were moved toward the membrane with constant velocity.

(B–D) The mean reaction force acting on the piston was calculated at three velocities: (B) 10^{-4} nm/ps for 40 ns, (C) 10^{-5} nm/ps for 300 ns, and (D) 10^{-6} nm/ps for 700 ns.

(E) Effective rigidity in the asymmetric and symmetric membrane at the indicated piston velocity was calculated from the molecular dynamics simulations.

(F) Intracellular distribution of actin cytoskeleton visualized by Lifeact-EGFP in Kc167 and XKR-deficient #122 cells treated with or without cytochalasin D (CytoD). Scale bar, 10 μm.

(G and H) Membrane tensions and Young's moduli of CytoD-treated Kc167 (n = 26) and XKR-deficient #122 (n = 19) cells.

(I) Localization of EGFP-XKR, LactC2-EGFP, Lifeact-EGFP, and EGFP-βH-spectrin in intact Kc167 cells and giant plasma membrane vesicles (GPMVs) isolated from Kc167 cells. Scale bar, 10 μm.

(J) Bending stiffness of GPMVs isolated from Kc167 (n = 12) and XKR-deficient #122 cells (n = 17) were calculated using flicker spectroscopy.

For boxplots, center mark is median, whiskers are minimum/maximum excluding outliers, and circles are outliers (G, H, and J). Mean ± SD (E). Student's t test (G, H, and J). *p < 0.05, **p < 0.01, ***p < 0.001.

of phospholipids enhances the deformability of the phospholipid bilayer.

XKR regulates the mechanical properties of the phospholipid bilayer

To evaluate the contribution of XKR to regulation of the mechanical properties of the phospholipid bilayer, we disrupted the actin cortex by cytochalasin D (CytoD) treatment (Figure 5F). Even in the absence of the actin cortex, the membrane tension and Young's modulus of Kc167 cells were increased by the depletion of XKR (Figures 5G and 5H), indicating that XKR could also enhance the deformation of the plasma membrane in a manner independent of the actin cytoskeleton. To more precisely evaluate the role of XKR in regulating the deformability of the phospholipid bilayer, we used giant plasma membrane vesicles (GPMVs) (Sezgin et al., 2012) that were isolated from the plasma membrane of *Drosophila* cells and lacked the actin cortex (Figure 5I). The micropipette aspiration experiment showed that

京都大学 KYOTO UNIVERSITY
A Self-archived copy in
Kyoto University Research Information Repository
https://repository.kulib.kyoto-u.ac.jp
京都大学学術情報リポジトリ KURENAI 紅 Kyoto University Research Information Repository

GPMVs isolated from XKR-deficient cells were less deformable than those from Kc167 cells (Figure S6B). We also measured the bending stiffness of GPMVs using flicker noise spectroscopy (Figures S6C and S6D) (Ito et al., 2015). The bending stiffness of GPMVs isolated from XKR-deficient cells was 1.8-fold higher than that of GPMVs isolated from wild-type cells (Figure 5J). These results demonstrated that the constitutive scrambling of phospholipids facilitated by XKR confers the high elastic deformability to the phospholipid bilayer of the plasma membrane.

Contribution of XKR to the deformation and resistance to fluid shear stress in *Drosophila* hemocytes

Drosophila has an open vasculature system in which the dorsal vessel pumps hemolymphs as well as hemocytes (blood cells) with rapid intravascular flow to circulate throughout the body cavity (Babcock et al., 2008; Choma et al., 2011; Curtis et al., 1999). Thus, we expected that *Drosophila* hemocytes have high deformability and resistance to pulsatile fluid shear stress caused by the rapid hemolymph flow. We investigated the role of XKR in the deformability and resistance to fluid shear stress, followed by assessment of its function in the *Drosophila* cardiovascular system. Cell deformability evaluated by the deformation index score in microchannel flow analysis (Figure 6A) demonstrated that the deformability of Kc167 cells was markedly decreased in the XKR-deficient cells (Figure 6B). Resistance to high fluid shear stress was also significantly reduced in the XKR-deficient Kc167 mutant cells and restored by the re-expression of XKR (Figure 6C).

Similar to *Drosophila* cell lines, hemocytes isolated from *Drosophila* larvae have a highly elastic cell membrane with remarkably low membrane tension (27.7 ± 7.8 pN/μm) and Young's modulus (19.3 ± 3.7 Pa), and defective expression of XKR via hemocyte-specific RNA interference significantly reduced the deformability of the isolated hemocytes (Figures 6D and 6E). Furthermore, hemocyte-specific suppression of XKR expression in *Drosophila* larvae led to a significant reduction in the number of circulating hemocytes relative to the number in the wild-type, whereas no significant change in the number of resident hemocytes that attached to the tissue surface was observed (Figure 6F). In *Drosophila* larvae, hemocytes enter the heart via the posterior and circulate anteriorly at speeds of ≤3.2 mm/s, corresponding to the rate of erythrocyte flow through vertebrate microvessels (Babcock et al., 2008). The observation of hemocyte dynamics in *Drosophila* larvae using GFP-expressed hemocytes demonstrated that circulating hemocytes were aggregated in the larval posterior by the defective expression of XKR, possibly because of the narrowed ostia at reentry into the heart (Figure 6G; Video S3). Thus, the XKR-mediated regulation of the mechanical properties of cell membranes is essential for the circulation of hemocytes in the cardiovascular system of *Drosophila*.

Enhanced deformation of cell membranes in animal cells expressing constitutive active phospholipid scramblases

Since the *Aedes* cell line C6/36 also showed higher deformability than did mammalian cells and the *Spodoptera frugiperda* cell line Sf9 (Figures 1B, 1D, and 1E), we isolated cDNA encoding a mosquito homolog of XKR (AaXKR) from C6/36 cells. Although AaXKR has relatively low homology with *Drosophila melanogaster* XKR (42.9% similarity, 26.5% identity), AaXKR also lacks a consensus motif for caspase recognition in either the N- or the C-terminal domains, similar to *Drosophila* XKR (Figure 3A). The deformation phenotypes of the XKR-deficient Kc167 mutant cells were completely rescued by the expression of AaXKR (Figures 2D, 2E, and S1D), demonstrating that the mosquito scramblase can also confer high deformability to the cell membranes.

We also examined whether the expression of XKR affects the deformability of mammalian cells. As expected, the expression of mouse Xkr8 in Chinese hamster-derived CHO-K1 cells had no significant effects on the membrane tension or Young's modulus (Figures 7A and 7B), because mammalian Xkr8 could be activated in apoptotic cells (Suzuki et al., 2013). Although *Drosophila* XKR expressed in CHO-K1 cells was not transported to the plasma membrane, AaXKR was transported to the plasma membrane in CHO-K1 cells (Figure 7C). The expression of AaXKR significantly decreased the membrane tension and Young's modulus in CHO-K1 cells (Figures 7A and 7B). Thus, the constitutive active phospholipid scramblases facilitate the deformation of cell membranes in mammalian cells, as well as in insect cells.

DISCUSSION

In this study, we found that small insects, such as the fruit fly and mosquito, have highly elastic cell membranes with extremely low membrane tension and high resistance to mechanical stress. Moreover, in contrast to all other eukaryotic cells, phospholipids are symmetrically distributed between the bilayer leaflets of the insect plasma membrane, where constitutive active phospholipid scramblase XKR bi-directionally transports phospholipids between leaflets of the bilayer membrane. As discussed below, XKR-facilitated phospholipid scrambling could promote the deformability of cell membranes by regulating actin cortex dynamics and mechanical properties of phospholipid bilayers. The membrane organization found in *Drosophila* may be advantageous to construct highly curved resilient membranes that enable development of the miniaturized organ systems of agile flying creatures.

In mammalian cells, the mechanical properties of cell membranes largely depend on the actin cytoskeleton (Fabry et al., 2003), as membrane tension of CHO-K1 cells was decreased 12.4-fold when the actin cytoskeleton was disassembled by CytoD treatment (Table S2). Alternatively, the membrane tension of Kc167 cells was decreased only 2.7-fold by CytoD treatment (Table S2), indicating that the actin cortex of *Drosophila* cells has distinct mechanical properties for constructing the highly deformable cell membranes. Chugh et al. (2017) reported that actin cortex thickness and membrane tension are inversely correlated during cell cycle progression in mammalian cells: the mitotic cells have a thin cortex with high cortical tension. In this study, we found that the actin cortex thickness of Kc167 cells was decreased by the depletion of XKR (Figure 4A). Moreover, the decrease of membrane tension by CytoD treatment in

京都大学 KYOTO UNIVERSITY
A Self-archived copy in
Kyoto University Research Information Repository
https://repository.kulib.kyoto-u.ac.jp
京都大学学術情報リポジトリ KURENAI 紅 Kyoto University Research Information Repository

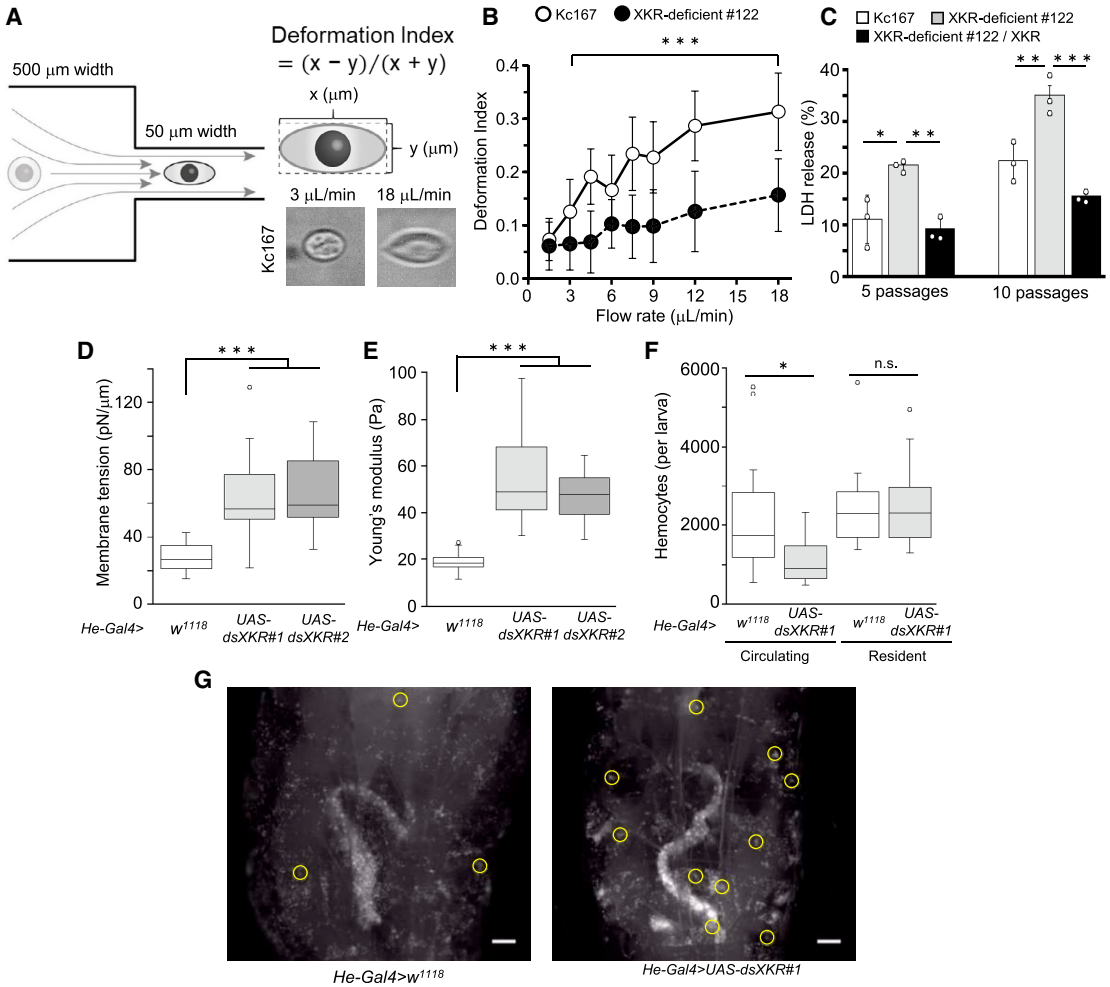

Figure 6. Role of XKR-mediated regulation of the mechanical properties of cell membranes in the cardiovascular system of *Drosophila*

(A) (Left) Structure of the microchannel. (Right) The deformation index was determined from the height (y) and width (x) of cells passed through a 50-μm-wide microchannel. Deformation of Kc167 cells at the indicated flow rate.

(B) Deformation index values in Kc167 (1.5–18 μL/min flow rate; n = 35, 97, 26, 81, 22, 35, 35, and 30) and XKR-deficient #122 (1.5–18 μL/min flow rate; n = 33, 100, 43, 79, 40, 50, 40, and 29) cells.

(C) Cells were passed through a narrow capillary (159-μm inner diameter, 12-mm length) at a constant flow rate (250 μL/s) 5 or 10 times and leakage of intracellular LDH into medium was analyzed.

(D and E) Membrane tensions and Young's moduli of hemocytes isolated from the third instar larva of He-Gal4>w^{1118} (n = 22), He-Gal4>UAS-dsXKR#1 (n = 22), and He-Gal4>UAS-dsXKR#2 (n = 21).

(F) Number of circulating and resident hemocytes isolated from the third instar larva of He-Gal4>w^{1118} (n = 20) and He-Gal4>UAS-dsXKR#1 (n = 20).

(G) EGFP-expressing hemocytes in the posterior end of the third instar larva of He-Gal4>w^{1118} and He-Gal4>UAS-dsXKR#1. Yellow circles indicate aggregated circulating hemocytes. Scale bar, 100 μm.

Mean ± SD (B and C). For boxplots, center mark is median, whiskers are minimum/maximum excluding outliers, and circles are outliers (D–F). Tukey's test (B–F). *p < 0.05, **p < 0.01, ***p < 0.001; n.s., not significant.

XKR-deficient cells was 1.3-fold higher than that in Kc167 cells (Table S2), showing that XKR regulates the mechanical properties of the actin cortex.

We identified Moe, a linker protein between the plasma membrane and actin cortex, as an effector in the XKR-mediated formation of highly deformable cell membranes. Moe is directly phosphorylated at a threonine residue in the C-terminal domain by Rho-associated kinase (RhoK) that regulates the dynamics of several cytoskeletal proteins (Matsui et al., 1998). The phosphorylated Moe is localized at the plasma membrane by enhanced binding of its N-terminal FERM domain to PI-4,5-bisphosphate (PIP_2), which causes the construction of a rigid cortical actin filament (Chishti et al., 1998; Fehon et al., 2010). We found that the expression of MoeTA decreased the membrane tension and Young's modulus of XKR-deficient cells, but not those of Kc167 cells (Figures 4B and 4C). Thus, it is likely that the Moe-mediated actin cortex stiffening is enhanced in XKR-deficient cells. However, the phosphorylation of Moe remained unchanged upon the depletion of XKR (Figures 4D). Conversely, turnover of EGFP-fused MoeTD and the FERM domain on the

京都大学 KYOTO UNIVERSITY
A Self-archived copy in
Kyoto University Research Information Repository
https://repository.kulib.kyoto-u.ac.jp
京都大学学術情報リポジトリ KURENAI 紅 Kyoto University Research Information Repository

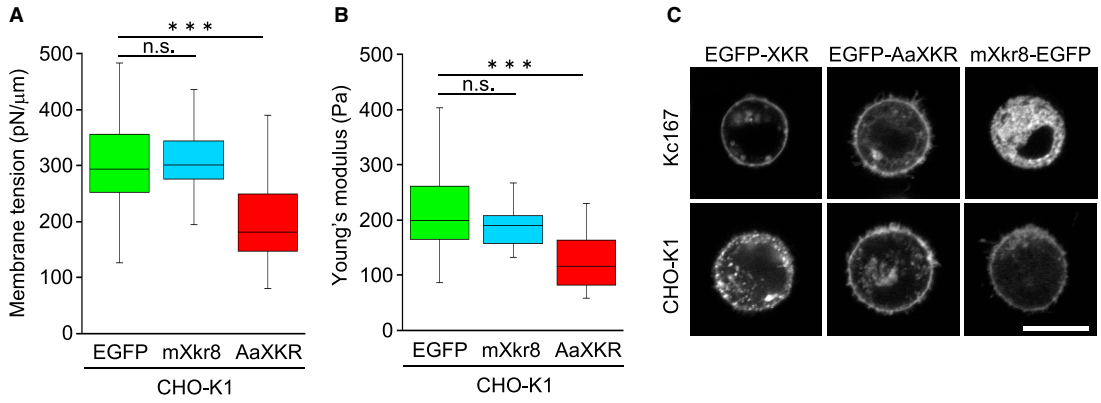

Figure 7. Constitutive active phospholipid scramblase facilitates the deformability of animal cell membranes

(A and B) Membrane tensions and Young's moduli of CHO-K1 cells expressing EGFP (n = 20), mXkr8-EGFP (n = 20), or EGFP-AaXKR (n = 24).

(C) Cellular localization of EGFP-XKR, EGFP-AaXKR, and mXkr8-EGFP in Kc167 and CHO-K1 cells. Scale bar, 10 μm.

For boxplots, center mark is median, whiskers are minimum/maximum excluding outliers, and circles are outliers (A and B). Tukey's test (A and B). ***p < 0.001; n.s., not significant.

plasma membrane was suppressed in XKR-deficient cells (Figures 4E, 4F, 4H, and 4I). Additionally, the proportion of MoeTD localized at the plasma membrane was increased by the depletion of XKR (Figure 4G). The distribution and lateral diffusion of PIP_2, a ligand of the FERM domain, on the surface of the plasma membrane were not changed by the depletion of XKR (Figures S5L and S5M). Because it is reported that PE molecules are laterally organized within monolayer via inter head group interaction (Pitman et al., 2005), it could be possible that trans-bilayer movement of PE molecules disturbs the lateral organization of PE molecules at the inner leaflet of the plasma membrane. Because primary amines of PE molecules also form hydrogen bonds with phosphomonoester of the anionic phospholipids, such as PIP_2 (Graber et al., 2012), we speculate that the XKR-facilitated lipid scrambling affects the interaction of PIP_2 molecules with the FERM domain of Moe by regulating the lipid environment at the inner surface of the plasma membrane, which may modulate the dynamics of the actin cortex to organize the highly deformable cell membranes.

Previous studies have reported that the symmetric distribution of phospholipid acyl chains in bilayer membrane reduces the rigidity compared with asymmetric membrane (Elani et al., 2015; Lu et al., 2016). However, the contribution of the trans-bilayer distribution of phospholipid head groups to the mechanical properties of phospholipid bilayers is not yet known. Using molecular dynamics simulations in which the micropipette aspiration assay was mimicked on much shorter time and smaller length scales, we showed that a symmetric membrane was more deformable than an asymmetric one (Figures 5A–5E). The bilayer coupling mechanism that regulates the domain formation in the bilayer membrane has been proposed to be applicable on a length scale up to micrometers (Schmid, 2017). Although simulation results are not directly comparable with aspiration experiments owing to different time and length scales, they suggest that a symmetrical distribution of phospholipids has an advantage for the construction of highly deformable cell membranes. We also showed that the depletion of XKR caused an increase of 2.9-fold in membrane tension even in the absence of the actin cytoskeleton (Figure 5G). Moreover, the bending stiffness of GPMVs, which lacked a cortical actin network (Figure 5I) (Keller et al., 2009), was increased by the depletion of XKR (Figure 5J), suggesting that *Drosophila* XKR also enhances elastic deformation of the phospholipid bilayer. Each leaflet of the plasma membrane bilayer is asymmetric in acyl chain composition of phospholipids. This asymmetry affects the stiffness of each leaflet (Lorent et al., 2020). Because PE and PC molecules have different acyl chain composition in *Drosophila* and mammalian cells (Figures S2D and S2E) (Lorent et al., 2020), modulation of trans-bilayer distribution of phospholipids by scramblase could affect acyl chain composition and stiffness of each leaflet of plasma membrane. Furthermore, PE molecules can interact with neighboring lipid molecules, thus forming a lateral membrane domain with enhanced ionization in the PE-rich membrane (Ogawa et al., 2015; Pitman et al., 2005). Because trans-bilayer transport of phospholipids affects both composition and dynamics of membrane lipids for each leaflet (Mioka et al., 2018; Panatala et al., 2015; Pomorski and Menon, 2006), membrane lipid interactions and domain formation might be regulated by phospholipid scrambling. Thus, the regulation of trans-bilayer movement and distribution of phospholipid molecules by scramblase might be advantageous for the formation of highly deformable phospholipid bilayers.

PE comprises a high proportion of total phospholipid of most insects (Past, 1971). PE constitutes more than half of membrane phospholipids in *Drosophila* (Carvalho et al., 2012; Marheineke et al., 1998; Past, 1971). We demonstrate that *Drosophila* cell lines also display high PE content (Table S1). Cone-shaped lipids, such as PE, favor non-bilayer structures, denoted by hexagonal II and cubic phases, and PE-rich membranes tend to exert bending fluctuations and generate intrinsic negative curvature (Chernomordik et al., 1995). Furthermore, *Drosophila* cells show lower sterol content than do mammalian cells (Carvalho et al., 2012; Dawaliby et al., 2016) (Table S3). Cholesterol content is a primary determinant of mechanical properties of bilayer membranes (Needham and Nunn, 1990). Thus, high PE/PC ratio and low cholesterol content in *Drosophila* cells would be

京都大学 KYOTO UNIVERSITY
A Self-archived copy in
Kyoto University Research Information Repository
https://repository.kulib.kyoto-u.ac.jp
京都大学学術情報リポジトリ KURENAI 紅 Kyoto University Research Information Repository

involved in the formation of the highly deformable membranes. However, phospholipid composition and cholesterol content in Kc167 cells were not changed by depletion in XKR (Tables S1 and S3). Furthermore, comparable compositions of PE and PC molecules were observed in XKR-deficient and XKR-rescued cells (Figures S2D and S2E). Thus, control of lipid composition of cell membranes is not involved in XKR-mediated regulation of cell deformability. Moreover, cellular deformability was enhanced by expression of AaXKR in CHO-K1 cells that are enriched in PC and cholesterol (Figures 7A and 7B). The lipid composition in *Drosophila* cells is an attractive research subject for future studies, but a high PE/PC ratio and low cholesterol content are likely not prerequisites for XKR-mediated regulation of cell deformability.

Although *Drosophila melanogaster* has provided a useful model system for a wide variety of biological studies, the basic molecular organization of its cellular system is not fully understood. Our findings suggest that *Drosophila* has evolved a membrane system in which XKR-facilitated lipid scrambling greatly enhances viscoelastic deformation. *Drosophila* XKR proteins lack the C-terminal domain that is removed by caspase-mediated cleavage in mammalian Xkr8 (Figures 3A and S7); that is, cleavage of the C-terminal domain is not required for phospholipid scrambling by *Drosophila* XKR. In fact, trans-bilayer transport of phospholipids was observed in living Kc167 cells and suppressed by the depletion of XKR (Figures 3D, 3E, S4E–S4G, S4I, and S4J). The structural features similar to those of *Drosophila* XKR in other small insects, such as the cat flea *Ctenocephalides felis* (XP_026467720), a species of solitary ground-nesting bee *Dufourea novaeangliae* (KZC09005), and a eusocial termite *Zootermopsis nevadensis* (XP_021921864) (Figure 3A), suggest that the constitutively active scramblase-mediated phospholipid organization and viscoelastic properties of cell membranes are widely conserved in various insect species.

Recently, it was reported that mouse Xkr8 can be activated by phosphorylation in living cells (Sakuragi et al., 2019), which raises the intriguing possibility that the local activation of the scramblase also changes the viscoelastic properties of mammalian cell membranes. Furthermore, the phospholipid scrambling by TMEM16 family members could be induced by calcium signaling in living cells (Suzuki et al., 2010). Because the deformability of mammalian cells was increased by the ectopic expression of AaXKR (Figures 7A and 7B), regulation of the elastic deformation of cell membranes by phospholipid scramblase is likely to occur in mammalian cells. Therefore, it would be intriguing to evaluate whether phospholipid scrambling by endogenous scramblases also regulates the deformability of mammalian cell membranes in specific cases in which PS exposure is observed (e.g., cancer cells, activated platelets, T cells, and B cells) (Lentz, 2003; Vallabhapurapu et al., 2015). Thus, our findings of the membrane lipid-mediated changes in the mechanical properties of cell membranes also provide insight into the pathophysiology of human diseases, such as cancer metastasis (Jain et al., 2014).

Limitations of the study

In this study, we demonstrated that XKR-facilitated phospholipid scrambling potentiates the deformability of cell membranes by regulating both actin cortex dynamics and mechanical properties of the phospholipid bilayer. Because XKR affects multiple steps in cell deformation, further experimentations are required to elucidate the integrated mechanism underlying the regulation of cell deformation by XKR.

We identified Moe, a linker protein connecting the plasma membrane and the actin cortex (Fehon et al., 2010), as an effector in the XKR-mediated regulation of cell deformation by analyzing the intracellular dynamics of Moe and the effect of Moe mutations on cell deformation (Figure 4). We revealed that Moe plays a dominant role in regulating cell deformation in Kc167 cells and that interaction of Moe with the plasma membrane is affected by the action of XKR in a manner independent of the control of Moe phosphorylation. However, since Moe is reported to regulate the mechanical properties of the cell membrane by cooperative actions with various cytoskeleton-related proteins, such as actin, spectrin, myosin, Arp2/3, and RhoK (Chugh et al., 2017; Luo et al., 2013), these functional interactions might also be involved in the XKR-mediated remodeling of the actin cortex for the construction of highly deformable cell membranes.

We found that the phospholipid bilayer's mechanical properties could be regulated by XKR (Figures 5 and S6). Because the actin cortex has a considerable contribution to the mechanical properties of the plasma membrane, we analyzed the mechanical properties of phospholipid bilayer by disrupting the actin cortex or isolating the plasma membrane fractions that lack actin cortex network. We also analyzed the effect of the trans-bilayer distribution of phospholipids on the deformation of bilayer membranes using molecular dynamics simulations. Although these approaches are widely used to evaluate the mechanical properties of phospholipid bilayer, these experiments have limitations in interpreting data relating to the deformation of intact cell membranes. Thus, although it is apparent that XKR-facilitated phospholipid scrambling regulates the mechanical properties of the phospholipid bilayer, quantitative evaluation of its contribution to the deformability of intact cell membranes is required in future studies. However, since the actin cortex and phospholipid bilayer are structurally and functionally interrelated in living cells, rigorous evaluation would be required.

XKR regulated membrane tension as well as Young's and bending moduli. The membrane tension of a uniform membrane is mainly set by the forces acting on the membrane, such as the transmembrane pressure difference. However, the membrane tension of intact cells is based on highly sophisticated feedback circuits, including the regulation of endocytosis, exocytosis, blebbing, and cytoskeleton rearrangement (Chugh et al., 2017; Matsui et al., 1998). Thus, the membrane tension of intact cells largely depends on the dynamics of cell membrane constituents. We showed that XKR changes the trans-bilayer distribution of phospholipids (Figures 2A–2C and S2C) and facilitates the scrambling of phospholipids (Figures 3D, 3E, and S4E–S4J). Moreover, we demonstrated that XKR regulates actin cortex dynamics via modulation of the Moe function (Figure 4). Therefore, it is likely that XKR regulates membrane tension by modulating the trans-bilayer distribution of phospholipids and cell membrane constituents' dynamics. However, there is an apparent gap between scrambling of lipid molecules and micrometer scale membrane dynamics, which hinder the simple elucidation of causal relationships. Further analysis using molecular sensors

京都大学 KYOTO UNIVERSITY
A Self-archived copy in
Kyoto University Research Information Repository
https://repository.kulib.kyoto-u.ac.jp
京都大学学術情報リポジトリ KURENAI 紅 Kyoto University Research Information Repository

of membrane dynamics, single molecular tracking of phospholipids, and molecular dynamics simulations on a micrometer scale will fill the gap.

STAR★METHODS

Detailed methods are provided in the online version of this paper and include the following:

- KEY RESOURCES TABLE
- RESOURCE AVAILABILITY
  - Lead contact
  - Materials availability
  - Data and code availability
- EXPERIMENTAL MODEL AND SUBJECT DETAILS
  - Fly stocks
  - Cell lines
- METHOD DETAILS
  - Construction of plasmids
  - RNA interference of *Drosophila* cells
  - Disruption of Xkr and Cdc50 genes in Kc167 cells
  - Aspiration of cells by capillary vessel
  - Micropipette aspiration assay
  - Intermittent high fluid shear stress assay
  - Isolation of plasma membranes
  - Analysis of cellular phospholipids and cholesterol
  - Mass spectrometric analysis of phospholipids
  - Induction of apoptosis
  - Staining of cell-surface PE and PS
  - Evaluation of cell surface exposure of PE and PS by flow cytometry
  - SDS-digested freeze-fracture replica labeling (SDS-FRL)
  - Electron microscopy observations of plasma membrane
  - Immunoblotting
  - Ro09-0198 cellular toxicity assay
  - NBD-labeled phospholipid incorporation assay
  - Analysis of actin cortex thickness
  - Preparation of giant plasma membrane vesicles (GPMVs)
  - Flicker spectroscopy of GPMVs
  - Cellular deformation analysis under microchannel flow
  - Fluorescence recovery after photobleaching assay
  - Isolation of circulating and resident hemocytes
  - Molecular dynamics simulations
- QUANTIFICATION AND STATISTICAL ANALYSIS

SUPPLEMENTAL INFORMATION

Supplemental information can be found online at https://doi.org/10.1016/j.celrep.2021.109219.

ACKNOWLEDGMENTS

We thank K. Akiyoshi, S. Sawada, H. Watanabe, Y. Matsumiya, T. Takigawa, J. Horinaka, S.H. Yoshimura, and A. Yoshida (Kyoto University) for valuable advice and technical assistance. This study was supported in part by Grants-in-Aid for Scientific Research on Innovative Areas (15H05930 to M.U.); the Fund for the Promotion of Joint International Research (15K21744 to M.U.); Grants-in-Aid for Scientific Research (KAKENHI) (25293012 and 17H03805 to M.U.; 15K07389 and 18K05433 to K. Nagao) from the Japan Society for the Promotion of Science (JSPS) and the Ministry of Education, Culture, Sports, Science and Technology (MEXT); a Grant-in-Aid for JSPS Research Fellow (17J09775 to A.S.); and by The Kyoto University Foundation (to K. Nagao). S.Y. was supported by the European Union's Horizon 2020 Research and Innovation Programme under the Marie Skłodowska-Curie Grant agreement no. 690853. The computational resources were provided by the Mésocentre de calcul de Franche-Comté.

AUTHOR CONTRIBUTIONS

M.U. conceived and designed the project. K. Nagao and M.U. supervised the research. A.S. performed most experiments with assistance from N.Y., M. Tsuchiya, U.K., N.J., Y.H., M.X.M., and Y.M. K.U.-T. established *Drosophila* cell lines. M.M. and T.K. performed SDS-FRL analysis. Y.N. and A.M. performed EM analysis. A.Y. and M. Tanaka performed Flicker spectroscopy. R.S., S.K., and M. Tanaka supervised biomechanical analysis. K.T., K. Nakabe, and H.S. supervised microchannel flow analysis. S.Y. and M.B. performed MD simulation analysis. A.S., K. Nagao, and M.U. interpreted data and wrote the manuscript.

DECLARATION OF INTERESTS

The authors declare no competing interests.

Received: August 18, 2020
Revised: April 2, 2021
Accepted: May 13, 2021
Published: June 8, 2021

REFERENCES

Albers, M.A., and Bradley, T.J. (2004). Osmotic regulation in adult *Drosophila melanogaster* during dehydration and rehydration. J. Exp. Biol. *207*, 2313–2321.

Aoki, Y., Uenaka, T., Aoki, J., Umeda, M., and Inoue, K. (1994). A novel peptide probe for studying the transbilayer movement of phosphatidylethanolamine. J. Biochem. *116*, 291–297.

Babcock, D.T., Brock, A.R., Fish, G.S., Wang, Y., Perrin, L., Krasnow, M.A., and Galko, M.J. (2008). Circulating blood cells function as a surveillance system for damaged tissue in *Drosophila* larvae. Proc. Natl. Acad. Sci. USA *105*, 10017–10022.

Barnes, J.M., Nauseef, J.T., and Henry, M.D. (2012). Resistance to fluid shear stress is a conserved biophysical property of malignant cells. PLoS ONE *7*, e50973.

Bassett, A.R., Tibbit, C., Ponting, C.P., and Liu, J.L. (2014). Mutagenesis and homologous recombination in *Drosophila* cell lines using CRISPR/Cas9. Biol. Open *3*, 42–49.

Bhat, H.B., Ishitsuka, R., Inaba, T., Murate, M., Abe, M., Makino, A., Kohyama-Koganeya, A., Nagao, K., Kurahashi, A., Kishimoto, T., et al. (2015). Evaluation of aegerolysins as novel tools to detect and visualize ceramide phosphoethanolamine, a major sphingolipid in invertebrates. FASEB J. *29*, 3920–3934.

Bligh, E.G., and Dyer, W.J. (1959). A rapid method of total lipid extraction and purification. Can. J. Biochem. Physiol. *37*, 911–917.

Brochard, F., and Lennon, J.F. (1975). Frequency spectrum of the flicker phenomenon in erythrocytes. J. Phys. (Paris) *36*, 1035–1047.

Carvalho, M., Sampaio, J.L., Palm, W., Brankatschk, M., Eaton, S., and Shevchenko, A. (2012). Effects of diet and development on the *Drosophila* lipidome. Mol. Syst. Biol. *8*, 600.

Charras, G.T., Hu, C.K., Coughlin, M., and Mitchison, T.J. (2006). Reassembly of contractile actin cortex in cell blebs. J. Cell Biol. *175*, 477–490.

Chernomordik, L., Kozlov, M.M., and Zimmerberg, J. (1995). Lipids in biological membrane fusion. J. Membr. Biol. *146*, 1–14.

京都大学 KYOTO UNIVERSITY
A Self-archived copy in
Kyoto University Research Information Repository
https://repository.kulib.kyoto-u.ac.jp
京都大学学術情報リポジトリ KURENAI 紅 Kyoto University Research Information Repository

Chishti, A.H., Kim, A.C., Marfatia, S.M., Lutchman, M., Hanspal, M., Jindal, H., Liu, S.C., Low, P.S., Rouleau, G.A., Mohandas, N., et al. (1998). The FERM domain: A unique module involved in the linkage of cytoplasmic proteins to the membrane. Trends Biochem. Sci. *23*, 281–282.

Choma, M.A., Suter, M.J., Vakoc, B.J., Bouma, B.E., and Tearney, G.J. (2011). Physiological homology between *Drosophila melanogaster* and vertebrate cardiovascular systems. Dis. Model. Mech. *4*, 411–420.

Chugh, P., Clark, A.G., Smith, M.B., Cassani, D.A.D., Dierkes, K., Ragab, A., Roux, P.P., Charras, G., Salbreux, G., and Paluch, E.K. (2017). Actin cortex architecture regulates cell surface tension. Nat. Cell Biol. *19*, 689–697.

Clark, A.G., Dierkes, K., and Paluch, E.K. (2013). Monitoring actin cortex thickness in live cells. Biophys. J. *105*, 570–580.

Coscoy, S., Waharte, F., Gautreau, A., Martin, M., Louvard, D., Mangeat, P., Arpin, M., and Amblard, F. (2002). Molecular analysis of microscopic ezrin dynamics by two-photon FRAP. Proc. Natl. Acad. Sci. USA *99*, 12813–12818.

Curtis, N.J., Ringo, J.M., and Dowse, H.B. (1999). Morphology of the pupal heart, adult heart, and associated tissues in the fruit fly, *Drosophila melanogaster*. J. Morphol. *240*, 225–235.

Dawaliby, R., Trubbia, C., Delporte, C., Noyon, C., Ruysschaert, J.-M., Van Antwerpen, P., and Govaerts, C. (2016). Phosphatidylethanolamine is a key regulator of membrane fluidity in eukaryotic cells. J. Biol. Chem. *291*, 3658–3667.

Diz-Muñoz, A., Fletcher, D.A., and Weiner, O.D. (2013). Use the force: membrane tension as an organizer of cell shape and motility. Trends Cell Biol. *23*, 47–53.

Elani, Y., Purushothaman, S., Booth, P.J., Seddon, J.M., Brooks, N.J., Law, R.V., and Ces, O. (2015). Measurements of the effect of membrane asymmetry on the mechanical properties of lipid bilayers. Chem. Commun. (Camb.) *51*, 6976–6979.

Emoto, K., Kobayashi, T., Yamaji, A., Aizawa, H., Yahara, I., Inoue, K., and Umeda, M. (1996). Redistribution of phosphatidylethanolamine at the cleavage furrow of dividing cells during cytokinesis. Proc. Natl. Acad. Sci. USA *93*, 12867–12872.

Emoto, K., Inadome, H., Kanaho, Y., Narumiya, S., and Umeda, M. (2005). Local change in phospholipid composition at the cleavage furrow is essential for completion of cytokinesis. J. Biol. Chem. *280*, 37901–37907.

Evans, E., and Needham, D. (1987). Physical properties of surfactant bilayer membranes: thermal transitions, elasticity, rigidity, cohesion and colloidal interactions. J. Phys. Chem. *91*, 4219–4228.

Fabry, B., Maksym, G.N., Butler, J.P., Glogauer, M., Navajas, D., Taback, N.A., Millet, E.J., and Fredberg, J.J. (2003). Time scale and other invariants of integrative mechanical behavior in living cells. Phys. Rev. E Stat. Nonlin. Soft Matter Phys. *68*, 041914.

Fehon, R.G., McClatchey, A.I., and Bretscher, A. (2010). Organizing the cell cortex: The role of ERM proteins. Nat. Rev. Mol. Cell Biol. *11*, 276–287.

Fritzsche, M., Thorogate, R., and Charras, G. (2014). Quantitative analysis of ezrin turnover dynamics in the actin cortex. Biophys. J. *106*, 343–353.

Gauthier, N.C., Masters, T.A., and Sheetz, M.P. (2012). Mechanical feedback between membrane tension and dynamics. Trends Cell Biol. *22*, 527–535.

Gov, N.S., and Safran, S.A. (2005). Red blood cell membrane fluctuations and shape controlled by ATP-induced cytoskeletal defects. Biophys. J. *88*, 1859–1874.

Graber, Z.T., Jiang, Z., Gericke, A., and Kooijman, E.E. (2012). Phosphatidylinositol-4,5-bisphosphate ionization and domain formation in the presence of lipids with hydrogen bond donor capabilities. Chem. Phys. Lipids *165*, 696–704.

Hanken, J., and Wake, D.B. (1993). Miniaturization of body-size—Organismal consequences and evolutionary significance. Annu. Rev. Ecol. Syst. *24*, 501–519.

Hess, B., Kutzner, C., van der Spoel, D., and Lindahl, E. (2008). GROMACS 4: Algorithms for highly efficient, load-balanced, and scalable molecular simulation. J. Chem. Theory Comput. *4*, 435–447.

Hochmuth, R.M. (2000). Micropipette aspiration of living cells. J. Biomech. *33*, 15–22.

Ito, H., Kuss, N., Rapp, B.E., Ichikawa, M., Gutsmann, T., Brandenburg, K., Pöschl, J.M., and Tanaka, M. (2015). Quantification of the influence of endotoxins on the mechanics of adult and neonatal red blood cells. J. Phys. Chem. B *119*, 7837–7845.

Jain, R.K., Martin, J.D., and Stylianopoulos, T. (2014). The role of mechanical forces in tumor growth and therapy. Annu. Rev. Biomed. Eng. *16*, 321–346.

Janmey, P.A., and Kinnunen, P.K.J. (2006). Biophysical properties of lipids and dynamic membranes. Trends Cell Biol. *16*, 538–546.

Jones, W.R., Ting-Beall, H.P., Lee, G.M., Kelley, S.S., Hochmuth, R.M., and Guilak, F. (1999). Alterations in the Young's modulus and volumetric properties of chondrocytes isolated from normal and osteoarthritic human cartilage. J. Biomech. *32*, 119–127.

Kammer, A.E., and Heinrich, B. (1978). Insect flight metabolism. Adv. Insect Physiol. *13*, 133–228.

Kato, U., Inadome, H., Yamamoto, M., Emoto, K., Kobayashi, T., and Umeda, M. (2013). Role for phospholipid flippase complex of ATP8A1 and CDC50A proteins in cell migration. J. Biol. Chem. *288*, 4922–4934.

Keller, H., Lorizate, M., and Schwille, P. (2009). $PI(4,5)P_2$ degradation promotes the formation of cytoskeleton-free model membrane systems. ChemPhysChem *10*, 2805–2812.

Kunda, P., Pelling, A.E., Liu, T., and Baum, B. (2008). Moesin controls cortical rigidity, cell rounding, and spindle morphogenesis during mitosis. Curr. Biol. *18*, 91–101.

Lee, Y.C., Block, G., Chen, H., Folch-Puy, E., Foronjy, R., Jalili, R., Jendresen, C.B., Kimura, M., Kraft, E., Lindemose, S., et al. (2008). One-step isolation of plasma membrane proteins using magnetic beads with immobilized concanavalin A. Protein Expr. Purif. *62*, 223–229.

Lentz, B.R. (2003). Exposure of platelet membrane phosphatidylserine regulates blood coagulation. Prog. Lipid Res. *42*, 423–438.

Lorent, J.H., Levental, K.R., Ganesan, L., Rivera-Longsworth, G., Sezgin, E., Doktorova, M.D., Lyman, E., and Levental, I. (2020). Plasma membranes are asymmetric in lipid unsaturation, packing and protein shape. Nat. Chem. Biol. *15*, 644–652.

Lu, L., Doak, W.J., Schertzer, J.W., and Chiarot, P.R. (2016). Membrane mechanical properties of synthetic asymmetric phospholipid vesicles. Soft Matter *12*, 7521–7528.

Luo, T., Mohan, K., Iglesias, P.A., and Robinson, D.N. (2013). Molecular mechanisms of cellular mechanosensing. Nat. Mater. *12*, 1064–1071.

Marheineke, K., Grünewald, S., Christie, W., and Reiländer, H. (1998). Lipid composition of *Spodoptera frugiperda* (Sf9) and Trichoplusia ni (Tn) insect cells used for baculovirus infection. FEBS Lett. *441*, 49–52.

Marrink, S.J., Risselada, H.J., Yefimov, S., Tieleman, D.P., and de Vries, A.H. (2007). The MARTINI force field: Coarse grained model for biomolecular simulations. J. Phys. Chem. B *111*, 7812–7824.

Matsui, T., Maeda, M., Doi, Y., Yonemura, S., Amano, M., Kaibuchi, K., Tsukita, S., and Tsukita, S. (1998). Rho-kinase phosphorylates COOH-terminal threonines of ezrin/radixin/moesin (ERM) proteins and regulates their head-to-tail association. J. Cell Biol. *140*, 647–657.

Matsuo, N., Nagao, K., Suito, T., Juni, N., Kato, U., Hara, Y., and Umeda, M. (2019). Different mechanisms for selective transport of fatty acids using a single class of lipoprotein in *Drosophila*. J. Lipid Res. *60*, 1199–1211.

McMahon, H.T., and Gallop, J.L. (2005). Membrane curvature and mechanisms of dynamic cell membrane remodelling. Nature *438*, 590–596.

Mioka, T., Fujimura-Kamada, K., Mizugaki, N., Kishimoto, T., Sano, T., Nunome, H., Williams, D.E., Andersen, R.J., and Tanaka, K. (2018). Phospholipid flippases and Sfk1p, a novel regulator of phospholipid asymmetry, contribute to low permeability of the plasma membrane. Mol. Biol. Cell *29*, 1203–1218.

Murakami, A., Nagao, K., Juni, N., Hara, Y., and Umeda, M. (2017). An N-terminal di-proline motif is essential for fatty acid-dependent degradation of Δ9-desaturase in *Drosophila*. J. Biol. Chem. *292*, 19976–19986.

京都大学 KYOTO UNIVERSITY
A Self-archived copy in
Kyoto University Research Information Repository
https://repository.kulib.kyoto-u.ac.jp
京都大学学術情報リポジトリ KURENAI 紅 Kyoto University Research Information Repository

Murate, M., Abe, M., Kasahara, K., Iwabuchi, K., Umeda, M., and Kobayashi, T. (2015). Transbilayer distribution of lipids at nano scale. J. Cell Sci. *128*, 1627–1638.

Naito, Y., Hino, K., Bono, H., and Ui-Tei, K. (2015). CRISPRdirect: Software for designing CRISPR/Cas guide RNA with reduced off-target sites. Bioinformatics *31*, 1120–1123.

Needham, D., and Nunn, R.S. (1990). Elastic deformation and failure of lipid bilayer membranes containing cholesterol. Biophys. J. *58*, 997–1009.

Ogawa, R., Nagao, K., Taniuchi, K., Tsuchiya, M., Kato, U., Hara, Y., Inaba, T., Kobayashi, T., Sasaki, Y., Akiyoshi, K., et al. (2015). Development of a novel tetravalent synthetic peptide that binds to phosphatidic acid. PLoS ONE *10*, e0131668.

Páll, S., Abraham, M.J., Kutzner, C., Hess, B., and Lindahl, E. (2015). Tackling exascale software challenges in molecular dynamics simulations with GROMACS. In Solving Software Challenges for Exascale. EASC 2014. Lecture Notes in Computer Science, volume 8759, S. Markidis and E. Laure, eds. (Springer), pp. 3–27.

Panatala, R., Hennrich, H., and Holthuis, J.C. (2015). Inner workings and biological impact of phospholipid flippases. J. Cell Sci. *128*, 2021–2032.

Past, P.G. (1971). Insect lipids. Prog. Chem. Fats Other Lipids *11*, 179–242.

Petraki, S., Alexander, B., and Brückner, K. (2015). Assaying blood cell populations of the *Drosophila melanogaster* larva. J. Vis. Exp. (*105*), 52733.

Pitman, M.C., Suits, F., Gawrisch, K., and Feller, S.E. (2005). Molecular dynamics investigation of dynamical properties of phosphatidylethanolamine lipid bilayers. J. Chem. Phys. *122*, 244715.

Polilov, A.A. (2015). Small is beautiful: Features of the smallest insects and limits to miniaturization. Annu. Rev. Entomol. *60*, 103–121.

Pomorski, T., and Menon, A.K. (2006). Lipid flippases and their biological functions. Cell. Mol. Life Sci. *63*, 2908–2921.

Pomorski, T.G., and Menon, A.K. (2016). Lipid somersaults: Uncovering the mechanisms of protein-mediated lipid flipping. Prog. Lipid Res. *64*, 69–84.

Roch, F., Polesello, C., Roubinet, C., Martin, M., Roy, C., Valenti, P., Carreno, S., Mangeat, P., and Payre, F. (2010). Differential roles of PtdIns(4,5)P_2 and phosphorylation in moesin activation during *Drosophila* development. J. Cell Sci. *123*, 2058–2067.

Rodriguez, M.L., McGarry, P.J., and Sniadecki, N.J. (2013). Review on cell mechanics: Experimental and modeling approaches. Appl. Mech. Rev. *65*, 1–41.

Roubinet, C., Decelle, B., Chicanne, G., Dorn, J.F., Payrastre, B., Payre, F., and Carreno, S. (2011). Molecular networks linked by Moesin drive remodeling of the cell cortex during mitosis. J. Cell Biol. *195*, 99–112.

Rouser, G., Siakotos, A.N., and Fleischer, S. (1966). Quantitative analysis of phospholipids by thin-layer chromatography and phosphorus analysis of spots. Lipids *1*, 85–86.

Sakuragi, T., Kosako, H., and Nagata, S. (2019). Phosphorylation-mediated activation of mouse Xkr8 scramblase for phosphatidylserine exposure. Proc. Natl. Acad. Sci. USA *116*, 2907–2912.

Salbreux, G., Charras, G., and Paluch, E. (2012). Actin cortex mechanics and cellular morphogenesis. Trends Cell Biol. *22*, 536–545.

Scheffers, B.R., Joppa, L.N., Pimm, S.L., and Laurance, W.F. (2012). What we know and don't know about Earth's missing biodiversity. Trends Ecol. Evol. *27*, 501–510.

Schmid, F. (2017). Physical mechanisms of micro- and nanodomain formation in multicomponent lipid membranes. Biochim. Biophys. Acta Biomembr. *1859*, 509–528.

Schneider, C.A., Rasband, W.S., and Eliceiri, K.W. (2012). NIH Image to ImageJ: 25 years of image analysis. Nat. Methods *9*, 671–675.

Sebastian, T.T., Baldridge, R.D., Xu, P., and Graham, T.R. (2012). Phospholipid flippases: Building asymmetric membranes and transport vesicles. Biochim. Biophys. Acta *1821*, 1068–1077.

Sezgin, E., Kaiser, H.-J., Baumgart, T., Schwille, P., Simons, K., and Levental, I. (2012). Elucidating membrane structure and protein behavior using giant plasma membrane vesicles. Nat. Protoc. *7*, 1042–1051.

Sheetz, M.P. (2001). Cell control by membrane-cytoskeleton adhesion. Nat. Rev. Mol. Cell Biol. *2*, 392–396.

Sheetz, M.P., and Singer, S.J. (1974). Biological membranes as bilayer couples. A molecular mechanism of drug-erythrocyte interactions. Proc. Natl. Acad. Sci. USA *71*, 4457–4461.

Sheetz, M.P., Painter, R.G., and Singer, S.J. (1976). Biological membranes as bilayer couples. III. Compensatory shape changes induced in membranes. J. Cell Biol. *70*, 193–203.

Sheetz, M.P., Sable, J.E., and Döbereiner, H.G. (2006). Continuous membrane-cytoskeleton adhesion requires continuous accommodation to lipid and cytoskeleton dynamics. Annu. Rev. Biophys. Biomol. Struct. *35*, 417–434.

Shiomi, A., Nagao, K., Kasai, H., Hara, Y., and Umeda, M. (2020). Changes in the physicochemical properties of fish cell membranes during cellular senescence. Biosci. Biotechnol. Biochem. *84*, 583–593.

Steinkühler, J., Sezgin, E., Urbančič, I., Eggeling, C., and Dimova, R. (2019). Mechanical properties of plasma membrane vesicles correlate with lipid order, viscosity and cell density. Commun. Biol. *2*, 337.

Suito, T., Nagao, K., Hatano, M., Kohashi, K., Tanabe, A., Ozaki, H., Kawamoto, J., Kurihara, T., Mioka, T., Tanaka, K., et al. (2018). Synthesis of omega-3 long-chain polyunsaturated fatty acid-rich triacylglycerols in an endemic goby, *Gymnogobius isaza*, from Lake Biwa, Japan. J. Biochem. *164*, 127–140.

Suzuki, J., Umeda, M., Sims, P.J., and Nagata, S. (2010). Calcium-dependent phospholipid scrambling by TMEM16F. Nature *468*, 834–838.

Suzuki, J., Denning, D.P., Imanishi, E., Horvitz, H.R., and Nagata, S. (2013). Xk-related protein 8 and CED-8 promote phosphatidylserine exposure in apoptotic cells. Science *341*, 403–406.

Tan, S.C., Pan, W.X., Ma, G., Cai, N., Leong, K.W., and Liao, K. (2008). Viscoelastic behaviour of human mesenchymal stem cells. BMC Cell Biol. *9*, 40.

Tatsumi, K., Haizumi, K., Sugimoto, K., and Nakabe, K. (2015). Measurement and analysis of lymphocyte deformation in microchannel contraction flows using a compound drop model. Flow Turbulence Combust. *96*, 245–260.

Tsuchiya, M., Hara, Y., Okuda, M., Itoh, K., Nishioka, R., Shiomi, A., Nagao, K., Mori, M., Mori, Y., Ikenouchi, J., et al. (2018). Cell surface flip-flop of phosphatidylserine is critical for PIEZO1-mediated myotube formation. Nat. Commun. *9*, 2049.

Vallabhapurapu, S.D., Blanco, V.M., Sulaiman, M.K., Vallabhapurapu, S.L., Chu, Z., Franco, R.S., and Qi, X. (2015). Variation in human cancer cell external phosphatidylserine is regulated by flippase activity and intracellular calcium. Oncotarget *6*, 34375–34388.

van Meer, G., Voelker, D.R., and Feigenson, G.W. (2008). Membrane lipids: Where they are and how they behave. Nat. Rev. Mol. Cell Biol. *9*, 112–124.

Vance, J.E. (2015). Phospholipid synthesis and transport in mammalian cells. Traffic *16*, 1–18.

Yesylevskyy, S.O. (2015). Pteros 2.0: Evolution of the fast parallel molecular analysis library for C++ and python. J. Comput. Chem. *36*, 1480–1488.

Yesylevskyy, S.O., Schäfer, L.V., Sengupta, D., and Marrink, S.J. (2010). Polarizable water model for the coarse-grained MARTINI force field. PLoS Comput. Biol. *6*, e1000810.

Yeung, T., Gilbert, G.E., Shi, J., Silvius, J., Kapus, A., and Grinstein, S. (2008). Membrane phosphatidylserine regulates surface charge and protein localization. Science *319*, 210–213.

京都大学 KYOTO UNIVERSITY
A Self-archived copy in
Kyoto University Research Information Repository
https://repository.kulib.kyoto-u.ac.jp
京都大学学術情報リポジトリ KURENAI 紅 Kyoto University Research Information Repository

STAR★METHODS

KEY RESOURCES TABLE

REAGENT or RESOURCE	SOURCE	IDENTIFIER
Antibodies		
HRP-conjugated goat polyclonal anti-rabbit IgG	Bethyl	Cat#A120-101P
HRP-conjugated goat polyclonal anti-mouse IgG	GE Healthcare	Cat#NA931
HRP-conjugated rabbit polyclonal anti-goat IgG	Santa Cruz Biotech	Cat#sc-2768
rabbit polyclonal anti-GM130	Abcam	Cat#Ab30637
rabbit polyclonal anti-NRV2.1	GeneTex	Cat#GTX124112
rabbit polyclonal anti-GFP	MBL	Cat#598
goat polyclonal anti-LMNA/C	Santa Cruz Biotech	Cat#sc6215
rabbit polyclonal anti-Flag (anti-DDDDK-tag)	MBL	Cat#PM020
mouse anti-Phospho-Threonine (42H4) IgM	Cell Signaling Technology	Cat#9386
rabbit polyclonal anti-SESB	This paper	N/A
rabbit polyclonal anti-DESAT1	Murakami et al., 2017	N/A
anti-Flag M2 Affinity Agarose Gel	Sigma-Aldrich	Cat#A2220
Chemicals, peptides, and recombinant proteins		
NBD-PE: 1-palmitoyl-2-{6-[(7-nitro-2-1,3-benzoxadiazol-4-yl)amino]hexanoyl}-sn-glycero-3-phosphoethanolamine	Avanti Polar Lipids	Cat#810153
NBD-PS: 1-palmitoyl-2-{6-[(7-nitro-2-1,3-benzoxadiazol-4-yl)amino]hexanoyl}-sn-glycero-3-phosphoserine	Avanti Polar Lipids	Cat#810192
NBD-PC: 1-palmitoyl-2-{6-[(7-nitro-2-1,3-benzoxadiazol-4-yl)amino]hexanoyl}-sn-glycero-3-phosphocholine	Avanti Polar Lipids	Cat#810130
FITC-conjugated streptavidin	Vector Laboratories	Cat#SA-5001
Fatty acid free BSA	Sigma-Aldrich	Cat#A6003
Ro09-0198	Aoki et al., 1994	N/A
Biotinylated Ro09-0198	Aoki et al., 1994	N/A
EGFP-Annexin V	PromoCell	Cat#PK-CA577-1004
FITC-Annexin V	MBL	Cat#4700-100
Cy5-Annexin V	PromoCell	Cat#PK-CA577-1013
TransFectin Lipid Reagent	BIO-RAD	Cat#1703350
ViaFect	PROMEGA	Cat#E4981
NucView 488 Caspase-3 Substrate	Biotium	Cat#10402
Critical commercial assays		
Cytotoxicity LDH assay kit-WST	DOJINDO	Cat#CK12
Super signal west pico	Thermo Fisher Scientific	Cat#34080
CellTiter 96 AQuousOne	PROMEGA	Cat#G3582
Cholesterol E-test	Wako	Cat#439-17501
In-Fusion HD cloning kit	Takara	Cat#639648
MEGAscript T7 transcription kit	Thermo Fisher Scientific	Cat#AMB13345
Experimental models: Cell lines		
D. melanogaster: Kc167 cells	Provided by Dr. Kumiko Ui-Tei	N/A
D. melanogaster: S2 cells	Provided by Dr. Kumiko Ui-Tei	N/A
D. melanogaster: BG3-c2 cells	Provided by Dr. Kumiko Ui-Tei	N/A
D. melanogaster: BG2-c2 cells	Provided by Dr. Kumiko Ui-Tei	N/A

(*Continued on next page*)

京都大学 KYOTO UNIVERSITY
A Self-archived copy in
Kyoto University Research Information Repository
https://repository.kulib.kyoto-u.ac.jp
京都大学学術情報リポジトリ KURENAI 紅 Kyoto University Research Information Repository

CellPress
OPEN ACCESS

Continued

REAGENT or RESOURCE	SOURCE	IDENTIFIER
D. melanogaster: BG2-c6 cells	Provided by Dr. Kumiko Ui-Tei	N/A
A. albopictus. C6/36 cells	JCRB	Cat#IFO50010, RRID:CVCL_Z230
Experimental models: organisms/strains		
D. melanogaster: w*; P{He-GAL4.Z}85, P{UAS-GFP.nls}8	Bloomington Drosophila Stock Center	BDSC: 8700 FlyBase: FBst0008700
D. melanogaster: y1 sc* v1 sev21; P{TRiP.HMC04978}attP40	Bloomington Drosophila Stock Center	BDSC: 57784 FlyBase: FBst0057784
D. melanogaster: w[1118]; P{GD15912}v48383	Vienna Drosophila Resource Center	VDRC: v48383 FlyBase: FBst0467884
D. melanogaster: y[1] w[*]; Pin[Yt] / CyO; P{w[+mC] = UAS-mCD8::GFP.L}LL6	KYOTO Stock Center	DGRC: 108061 FlyBase: FBst0306707
Oligonucleotides		
For Primer list see Table S4	This paper	N/A
Recombinant DNA		
cDNA *Xkr*	Drosophila Genomics Resource Center	LD13628 FlyBase:FBcl 0153079
cDNA *Moe*	Drosophila Genomics Resource Center	GH10189 FlyBase:FBcl 0119197
cDNA *Rlc*	Drosophila Genomics Resource Center	LD22691 FlyBase:FBcl 0163637
cDNA *Sqh*	Drosophila Genomics Resource Center	LD14743 FlyBase:FBcl 0151306
cDNA *Jaguar*	Drosophila Genomics Resource Center	RE25996 FlyBase:FBcl 0212495
cDNA *Rho1*	Drosophila Genomics Resource Center	GH20776 FlyBase:FBcl 0114647
cDNA *Lasp*	Drosophila Genomics Resource Center	AT23571 FlyBase:FBcl 0011567
Xkr8 (NM_201368) mouse tagged ORF clone	ORIGENE	Cat#MR206296
Plasmid: pAc5.1-V5-His-A	Thermo fisher scientific	Cat#V411020
Plasmid: pIRES-puro3	Takara	Cat#631619
Plasmid: pAc-sgRNA-Cas9	Bassett et al., 2014	Addgene Plasmid #49330
Plasmid: Lact-C2-GFP	Yeung et al., 2008	Addgene Plasmid #22852
Plasmid: PH-PLCδ1	Emoto et al., 2005	N/A
Software and algorithms		
ImageJ	Schneider et al., 2012	https://imagej.nih.gov/ij/
ZEN	Carl-Zeiss	https://www.zeiss.co.jp/corporate/home.html
Origin pro	Origin Labs	https://www.originlab.com
JMP11	SAS Institute	https://www.jmp.com/en_us/home.geo.html
FlowJo	BD Biosciences	https://www.flowjo.com
CellProfiler	Broad Institute	https://cellprofiler.org
Igor Pro	Wave Metrics	https://www.wavemetrics.com
Martini 2.2	Marrink et al., 2007	http://cgmartini.nl/index.php/224-m22
Gromacs 2018.2	Hess et al., 2008	https://manual.gromacs.org/documentation/2018.2/index.html
Pteros molecular modeling library	Yesylevskyy, 2015	https://yesint.github.io/pteros/

RESOURCE AVAILABILITY

Lead contact

Further information and requests for resources and reagents should be directed to and will be fulfilled by the Lead Contact, Masato Umeda (umeda@sbchem.kyoto-u.ac.jp).

Materials availability

All expression plasmids and reagents will be shared upon request.

京都大学 KYOTO UNIVERSITY
A Self-archived copy in
Kyoto University Research Information Repository
https://repository.kulib.kyoto-u.ac.jp
京都大学学術情報リポジトリ KURENAI 紅 Kyoto University Research Information Repository

Data and code availability

All data generated and analyzed in this study are available from the corresponding author on request. The custom compute codes used to generate results in this study are available from the corresponding author on request.

EXPERIMENTAL MODEL AND SUBJECT DETAILS

Fly stocks

Drosophila melanogaster was reared on standard medium containing glucose, brewer's yeast extract, corn meal, and agar, supplemented with propionic acid and butyl p-hydroxybenzoate for preservation at 25°C under a 12-h light/12-h dark cycle. The w^{1118} strain was obtained from the KYOTO Stock Center. He-GAL4 (8700) and UAS-dsXKR#1 (HMC04978) strains were obtained from the Bloomington *Drosophila* Stock Center. The UAS-dsXKR#2 (v48383) strain was obtained from the Vienna *Drosophila* Resource Center.

Cell lines

Drosophila Kc167 and S2 cells were cultured in Schneider's *Drosophila* medium (Thermo Fisher Scientific) supplemented with 10% (v/v) fetal bovine serum (FBS; Biowest) and penicillin-streptomycin (Wako) at 25°C. *Drosophila* BG3-c2, BG2-c2, and BG2-c6 cells were maintained in Schneider's *Drosophila* medium supplemented with 10% FBS, human insulin (Sigma-Aldrich), and penicillin-streptomycin (Wako) at 25°C. Mosquito C6/36 cells were maintained in Eagle's minimum essential medium (Wako) supplemented with 10% FBS at 28°C under an atmosphere containing 5% CO_2. Sf9 cells were grown as a suspension culture in Sf900 III SFM (Thermo Fisher Scientific) supplemented with pluronic F-68 (Thermo Fisher Scientific) at 26°C. All mammalian cell lines were maintained in medium supplemented with 10% FBS and penicillin-streptomycin at 37°C under an atmosphere containing 5% CO_2. Nutrient mixture F-12 HAM medium (Sigma-Aldrich) was used for the cultivation of CHO-K1 cells. RPMI-1640 medium (Sigma-Aldrich) was used for the cultivation of THP-1 and PC3 cells. Dulbecco's modified Eagle's medium (Thermo Fisher Scientific) was used for the cultivation of HeLa and Eph4 cells.

METHOD DETAILS

Construction of plasmids

The coding sequence of the *Egfp* gene was inserted into pAc5.1-V5-His-A (Thermo Fisher Scientific) to construct pAc5.1-N-EGFP and pAc5.1-C-EGFP, respectively. The coding sequence of *Drosophila* XKR (NM_167501) was obtained from *Drosophila* Genomics Resource Center (DGRC) (LD13628). The coding sequence of the *Xkr* gene was inserted into pAc5.1-N-EGFP and pAc5.1-C-EGFP to construct N-terminally and C-terminally EGFP-fused XKR expression plasmids, respectively. The coding sequence of *Aedes albopictus Xkr* (XM_019678113.1) was PCR-amplified from a cDNA library of C6/36 cells using specific primers (5′-CCGCTCGAGATG CAGGAAAAATTACCTACA-3′ and 5′-ATACTCGAGTTACTTGCTTGCGCCGGAA-3′) and ligated into pAc5.1-N-EGFP to construct pAc5.1-EGFP-AaXKR. The coding sequence of mouse *Xkr8* (NM_201368) was purchased from ORIGENE (MR206296) and inserted into pAc5.1-C-EGFP to construct pAc5.1-mXkr8-EGFP. Each coding sequence for EGFP-XKR, EGFP-AaXKR, or mXkr8-EGFP was inserted into pIRES-puro3 (Takara). For construction of pAc5.1-Lifeact-EGFP, synthetic oligonucleotides encoding the protein sequence MGVADLIKKFESISKEE were inserted into pAc5.1-C-EGFP in which an initiation methionine of the *Egfp* gene was replaced with alanine. The coding sequence of the LactC2-EGFP was PCR-amplified from a plasmid obtained from Addgene (Plasmid#22852), and then inserted into pAc5.1-V5-His-A to construct pAc5.1-LactC2-EGFP. The coding sequence of the β_h*-spectrin* gene (NM_001274439) was PCR-amplified from a cDNA library of *Drosophila* w^{1118} strain, and ligated into pAc5.1-N-EGFP using In-Fusion HD Cloning kit (Takara) to construct pAc5.1-EGFP-β_h-spectrin. The coding sequence of *Drosophila Moe* gene (RA variant; NM_167169) was obtained from DGRC (GH10189). The coding sequence of the Moe RA variant was converted to the Moe RJ variant (NM_206664) by deleting the nucleotides encoding amino acid residues 75–127, and replacing the sequence encoding amino acid residues 2–14 with the sequence encoding the four-amino-acid peptide SPKA, by using synthetic oligonucleotides and the In-Fusion HD Cloning kit. The coding sequence of Moe RJ variant was ligated into pAc5.1-C-EGFP to construct pAc5.1-Moe-EGFP. Threonine-559 encoded by the Moe RJ variant was replaced with alanine or aspartic acid to obtain pAc5.1-MoeTA-EGFP and pAc5.1-MoeTD-EGFP, respectively. To obtain pAc5.1-FERM domain-EGFP, the sequence encoding the C-terminal ERM-associated domain (C-ERMAD) (amino acid residues 483–578) was removed from pAc5.1-Moe-EGFP using the In-Fusion HD Cloning kit. The coding sequence of CD8 was PCR-amplified from a cDNA library of *Drosophila* strain obtained from the KYOTO Stock Center (108061). The coding sequences for CD8 and mRuby2 were inserted into pAc5.1-V5-His-A to construct pAc5.1-CD8-mRuby2. The coding sequence of *Drosophila* cytoskeleton associated proteins obtained from DGRC (RLC, LD22691; Sqh, LD14743; Jaguar, RE25996; Rho1, GH20776; Lasp, AT23571) were inserted into pAc5.1-N-EGFP and pAc5.1-C-EGFP to construct pAc5.1-RLC-EGFP, pAc5.1-Sqh-EGFP, pAc5.1-EGFP-Jaguar, pAc5.1-EGFP-Rho1, and pAc5.1-Lasp-EGFP, respectively. The coding sequence of the *Zipper* gene (NM_079136) was PCR-amplified from a cDNA library of *Drosophila* w^{1118} strain, and ligated into pAc5.1-N-EGFP using the In-Fusion HD Cloning kit to construct pAc5.1-EGFP-Zipper. The coding sequence of PH-PLCδ1 (Emoto et al., 2005) was ligated into pAc5.1-V5-His-A together with the coding sequence of mClover. Expression plasmids were introduced into Kc167 and CHO-K1 cells using TransFectin Lipid Reagent (BIO-RAD) and ViaFect (PROMEGA), respectively. To establish stable cell lines, pCo-Blast plasmid (Thermo Fisher Scientific) was co-transfected with pAc5.1 plasmids harboring genes of interest.

京都大学 KYOTO UNIVERSITY
A Self-archived copy in
Kyoto University Research Information Repository
https://repository.kulib.kyoto-u.ac.jp
京都大学学術情報リポジトリ KURENAI 紅 Kyoto University Research Information Repository

Transfected cells were observed with an LSM800 confocal microscope (Carl-Zeiss). Intracellular distribution and expression level of EGFP-fused proteins were analyzed using CellProfiler software (Broad Institute).

RNA interference of *Drosophila* cells

RNA interference (RNAi) in *Drosophila* Kc167 cells was performed as described previously (Bhat et al., 2015). dsRNA was synthesized by *in vitro* transcription of PCR products flanked by T7 RNA polymerase-binding sites using the MEGAscript T7 transcription kit (Thermo Fisher Scientific). Templates with a T7 promoter flanking both sides were amplified using specific primers (Table S4). *Drosophila* Kc167 cells were plated in a 35-mm dish and incubated with 30 μg dsRNA in 1 mL of serum-free Schneider's *Drosophila* medium for 1 h at 25°C. After adding 1 mL of Schneider's *Drosophila* medium supplemented with 20% (v/v) FBS, cells were incubated for 3 days at 25°C.

Disruption of Xkr and Cdc50 genes in Kc167 cells

XKR-deficient and CDC50-deficient *Drosophila* Kc167 cells were established using Clustered Regularly Interspaced Short Palindromic Repeats (CRISPR)/CRISPR-associated (Cas)9 gene editing. Target sequences within the genes of interest were designed using CRISPRdirect (Naito et al., 2015) and ligated into the pAc-sgRNA-Cas9 plasmid (Bassett et al., 2014) (#49330; Addgene) using synthetic oligonucleotides (XKR #122: 5′-TTCGGGAGCCTGGCGTACGTGTAC-3′ and 5′-AACGTACACGTACGCCAGGCTCCC-3′; XKR #160: 5′-TTCGGGATACTGCGCCTGGACCAT-3′ and 5′-AACATGGTCCAGGCGCAGTATCCC-3′; CDC50: 5′-TTCGGGAGAATGAGGAGAGTGCAG-3′ and 5′-AACCTGCACTCTCCTCATTCTCCC-3′). The pAc-sgRNA-Cas9 plasmid harboring specific target sequence was introduced into Kc167 cells. After two weeks of puromycin selection (5 μg/mL), single cell clones were isolated by limiting dilution. DNA sequencing was then used to identify mutations introduced into target genes within the genomes of cells.

Aspiration of cells by capillary vessel

A capillary vessel with < 1 μm inner diameter was manufactured from borosilicate glass capillaries (B150-86-10; Sutter Instruments) using a P-97 Micropipette Puller (Sutter Instruments). The tip of the capillary vessel was polished with MF-830 Microforge (Narishige). Cells (5×10^4) were washed twice with phosphate-buffered saline (PBS) containing 0.01% bovine serum albumin (BSA; Sigma-Aldrich), resuspended in 3 mL of PBS containing 0.01% BSA and incubated for 10 min in non-coated glass bottom dishes (MetTek). Cells were aspirated using the capillary vessel at 50 mmHg suction pressure for 120 s. The aspirated volume was calculated from changes in the cell diameter during aspiration using AxioVision software (Carl-Zeiss).

Micropipette aspiration assay

A 60-mm FluoroDish (World Precision Instruments) was coated with agarose (Iwai Chemicals) to prevent cell adhesion. Micropipettes were manufactured from borosilicate glass capillaries using a PC-10 Puller (Narishige) and then polished using Microforge (Narishige). Cells were washed with PBS and suspended in PBS containing 0.01% BSA, and then maintained for 10 min on the agarose-coated FluoroDish. Cells were aspirated with a micropipette under a series of increasing hydrostatic pressures created using adjustable water reservoirs. Aspirated length was measured at each pressure after a 60 s equilibration period using ZEN software (Carl-Zeiss).

The membrane tension was calculated from the experimental data using Equation 1 (Hochmuth, 2000) where T_c, ΔP_c, L, a, and R represent the membrane tension, the critical pressure, protrusion length, the inner radius of the pipette, and cell radius, respectively (Figure 1C).

$$T_c = \Delta P_c \Big/ 2\left(\frac{1}{a} - \frac{1}{R}\right), \ (\Delta \mathrm{P} = \Delta \mathrm{Pc \ when \ L \ = \ a}) \qquad \text{(Equation 1)}$$

The membrane tension is inter-related to the transmembrane pressure. The transmembrane pressure of cell is mainly determined by osmotic concentrations of cytosol and extracellular environment. The osmotic concentration of *Drosophila* hemolymph is reported to be 353 mOsm (Albers and Bradley, 2004), which is comparable to that of human serum. Schneider's *Drosophila* Medium that is used for cultivation of *Drosophila* cell lines also has comparable osmotic concentration (360 mOsm), that is similar to the osmotic concentration of culture medium for mammalian cell lines such as DMEM and Ham's F12. Thus, the effect of difference in the transmembrane pressure on the measurement of membrane tension is likely to be negligible in our experimental conditions.

Young's modulus in each cell was calculated using Equation 2 (Jones et al., 1999) where Young's modulus (E) depends on the suction pressure (ΔP) and the ratio of the inner radius of the pipette (a) to aspiration length (L). $\Phi(\eta)$ is defined as the wall function. $\eta = (b-a)/a$, where b represents the outer radius of pipette. A typical value for $\Phi(\eta)$ is reported to be ≈2.1. A constant suction pressure was applied to cells for at least 60 s until deformation of the cell stopped, and protrusion length and suction pressure was measured. Measurement was continuously recorded eight to ten times per cell by increasing suction pressure. A first-order approximation was used to obtain the ratio of suctioned length to suction pressure (ΔP/L).

$$E = \frac{3a\Delta P\Phi(\eta)}{2\pi L} \qquad \text{(Equation 2)}$$

京都大学 KYOTO UNIVERSITY
A Self-archived copy in
Kyoto University Research Information Repository
https://repository.kulib.kyoto-u.ac.jp
京都大学学術情報リポジトリ KURENAI 紅 Kyoto University Research Information Repository

The membrane tension and Young's modulus for each cell were calculated from experimental data using OriginPro software (OriginLab).

To measure the membrane tension and Young's modulus in the absence of cytoskeleton, cells were treated with 1 μM cytochalasin D (CytoD; Wako) and rotated for 30 min at room temperature. CytoD-treated cells were mixed with equal volumes of hypotonic PBS (10 mM Na_2HPO_4, 1.76 mM KH_2PO_4, 2.7 mM KCl) to maintain spherical cell shape. The disruption of the actin cytoskeleton by CytoD was evaluated by the cellular localization of Lifeact-EGFP.

Intermittent high fluid shear stress assay

Resistance of cells against high fluid shear stress was assayed as described previously (Barnes et al., 2012). Cells were washed with PBS containing 2.5 mM $CaCl_2$ and 2.5 mM $MgCl_2$, and then suspended in PBS. 5 mL of suspension (5×10^6 cells) was placed in a 10-mL syringe (TERUMO) equipped with a 30-gauge needle (HS-2739A; Dentronics) and was then expelled at a constant flow rate of 250 μL/s using a micro-syringe pump (KD Scientific). This process was repeated five or ten times and 100 μL aliquots were transferred to the 96-well plate. Lactate dehydrogenase (LDH) release induced by high fluid shear stress was measured using a Cytotoxicity LDH Assay Kit-WST (DOJINDO).

Isolation of plasma membranes

The isolation of plasma membranes was performed as described previously (Lee et al., 2008). Concanavalin A (ConA)-coupled magnetic beads were prepared by incubating Dynabeads M-280 Streptavidin (Thermo Fisher Scientific) with PBS containing 0.5 mg/mL of biotinylated ConA (Sigma-Aldrich) for 1 h. Unbound biotinylated ConA was removed by washing the beads with 1 mL of PBS containing 1% Triton X-100 three times and 1 mL of PBS three times. Cells (1×10^9) were washed three times with PBS and suspended in 900 μL of PBS. Glass beads (425–600 μm diameter; Sigma-Aldrich) were added to cell suspensions. The cell suspension was mixed using a vortex mixer for 30 s and kept on ice for 30 s. This homogenization process was repeated ten times. The cell homogenate was mixed with 5 mg of ConA-coupled magnetic beads in a 1.5 mL tube and rotated for 1 h at 4°C. The magnetic beads were precipitated with a magnet and gently washed with 500 μL of cold PBS five times. The magnetic beads were then incubated in 100 μL of PBS containing 0.25 M methyl α-D-mannopyranoside for 10 min to elute plasma membrane fractions. The elution step was repeated five times. To confirm the enrichment of plasma membranes, equal amounts of protein from total cell lysates, unbound fraction, and eluate fraction were analyzed using immunoblotting.

Analysis of cellular phospholipids and cholesterol

Cellular total lipids were extracted using the Bligh & Dyer method (Bligh and Dyer, 1959) and dissolved in chloroform. Phosphatidylcholine (PC), phosphatidylethanolamine (PE), phosphatidylserine (PS), phosphatidylinositol (PI), sphingomyelin (SM), and ceramide phosphoethanolamine (CerPE) were separated from the total lipid extract with two-dimensional thin layer chromatography (2D-TLC) using a first solvent system of chloroform/methanol/acetic acid (65:25:10, v/v/v) and a second solvent system of chloroform/methanol/formic acid (65:25:10, v/v/v) on a silica plate. The amount of phospholipid in each spot was determined by inorganic phosphate quantification (Rouser et al., 1966). The amount of cholesterol was determined by using Cholesterol E-test (Wako).

Mass spectrometric analysis of phospholipids

LC-MS/MS analysis was performed as previously reported (Matsuo et al., 2019; Suito et al., 2018). Analysis of PE and PC used LC-30AD high-performance liquid chromatography (Shimadzu) coupled to a triple quadrupole mass spectrometer LC-MS-8040 (Shimadzu) equipped with an electrospray source. Separation used a Kinetex C8 column (2.6 μm, 2.1 × 150 mm) (Phenomenex). A binary mobile phase used 10 mM NH_4HCO_2 in water (mobile phase A) and 10 mM NH_4HCO_2 in 2-propanol/acetonitrile/water (45:45:10, v/v/v) (mobile phase B). The gradient of mobile phase B was programmed as: an initial isocratic flow at 20% B for 1 min, a linear increase to 40% B for 1 min, an increase to 92.5% B using a curved gradient for 23 min, a linear increase to 100% B for 1 min, and a hold at 100% B for 4 min. The flow rate was 0.3 mL/min, column temperature was 45°C, and sample temperature was 4°C. The parameters for the spectrophotometer were: nebulizer gas flow 2 L/min, drying gas flow 15 L/min, interface voltage 4.5 kV, DL temperature 250°C, and heating block temperature 400°C. Multiple reaction monitoring transition was $[M+H]^+ \rightarrow [M + H–141.0]^+$ for PE and $[M+H]^+ \rightarrow [184.1]^+$ for PC.

Induction of apoptosis

To induce apoptosis, Kc167 cells or CHO-K1 cells were incubated with 3 μM actinomycin D (Sigma-Aldrich) at 25°C for 6 h or at 37°C for 12 h, respectively. To evaluate the induction of apoptosis, cells were incubated in PBS containing 0.1% BSA, 5 μM NucView 488 (Biotium), and 1 μg/mL Hoechst 33342 for 30 min. The cells were fixed in 4% paraformaldehyde at room temperature for 30 min and then observed with an LSM800 confocal microscope (Carl-Zeiss). Cells whose nuclei stained with NucView 488 were regarded as having undergone apoptosis.

Staining of cell-surface PE and PS

FITC-SA-Ro was prepared from FITC-conjugated streptavidin (Vector Laboratories) and biotinylated Ro09-0198 (Aoki et al., 1994). Cells were incubated on a poly-L-lysine coated cover glass for 1 h and washed three times with PBS. To detect PE in the outer leaflet

京都大学 KYOTO UNIVERSITY
A Self-archived copy in
Kyoto University Research Information Repository
https://repository.kulib.kyoto-u.ac.jp
京都大学学術情報リポジトリ KURENAI 紅 Kyoto University Research Information Repository

of plasma membranes, cells were washed with PBS containing 0.5% BSA (fatty acid free, Sigma-Aldrich) and then incubated for 30 min on ice in PBS containing 0.5% BSA and 10 μg/mL FITC-SA-Ro. After washing with ice-cold PBS containing 0.5% BSA, cells were observed with an LSM800 confocal microscope (Carl-Zeiss). To detect PS in the outer leaflet of plasma membranes, cells were incubated for 10 min in Annexin V staining buffer (10 mM Tris, pH7.4, 140 mM NaCl, 2.5 mM $CaCl_2$) containing 100-fold-diluted EGFP-Annexin V (PromoCell) at room temperature. After washing with Annexin V staining buffer, cells were observed with an LSM800 confocal microscope (Carl-Zeiss). To induce the externalization of PE and PS, CHO-K1 cells were treated with actinomycin D before incubation with FITC-SA-Ro and EGFP-Annexin V.

Evaluation of cell surface exposure of PE and PS by flow cytometry

To detect PE at the outer leaflet of plasma membranes, cells were washed with PBS containing 0.5% BSA (fatty acid free, Sigma-Aldrich) and then incubated for 30 min on ice in PBS containing 0.5% BSA, 5 μg/ml Propidium Iodide (PI), and 10 μg/mL FITC-SA-Ro. After washing with ice-cold PBS containing 0.5% BSA, cells were analyzed with a Cytomics FC500 instrument (Beckman). To detect PS at the outer leaflet of plasma membranes, cells were incubated for 10 min in Annexin V staining buffer containing 5 μg/ml PI and 100-fold-diluted FITC-Annexin V (PromoCell) or Cy5-Annexin V at room temperature. After washing with Annexin V staining buffer, cells were measured by a Cytomics FC500 instrument (Beckman) and analyzed with FlowJo (BD). PI-positive cells were excluded from analysis.

SDS-digested freeze-fracture replica labeling (SDS-FRL)

SDS-FRL was performed as previously reported (Murate et al., 2015). PE was labeled with biotinylated duramycin, followed by 15 nm gold-conjugated anti-biotin antibody (British BioCell International). PS was stained with mouse anti-PS monoclonal antibody (clone 1H6), followed by 10 nm gold-conjugated anti-mouse IgM (British BioCell International). Specimens were observed using transmission electron microscopy JEM1230 (JEOL). Electron micrographs were recorded with a Veleta charge-coupled device camera (Olympus Soft Imaging Solutions).

Electron microscopy observations of plasma membrane

Kc167 cells (1×10^7 cells) were washed with Tris-buffered saline (TBS) and suspended in TBS containing 20% dextrin. The cell suspensions were frozen under 210 MPa using an EM HPM100 high-pressure freezer (Leica Microsystems). The frozen cell suspension was then freeze-substituted into acetone containing both 1.0% osmium tetroxide and 0.2% uranyl acetate using an EM AFS2 freeze substitution system (Leica Microsystems). The samples were embedded in Epon 812 resin (TAAB Labs), and sectioned with 50 μm thickness using an EM UC7 ultramicrotome (Leica Microsystems). The ultrathin sections were stained with uranyl acetate and lead citrate. The plasma membranes of Kc167 cells were observed with a transmission electron microscope, JEM-2100, (JEOL) operating at an accelerating voltage of 200 kV.

Immunoblotting

Cells or membrane fractions were lysed in 20 mM Tris buffer (pH 7.5) containing 1% Triton X-100, 0.1% SDS, 1% sodium deoxycholate, 150 mM NaCl, and EDTA-free protease inhibitor (Nacalai Tesque). The lysates were centrifuged at 15,000 *g* for 5 min at 4°C. Fifteen microliters of lysate was mixed with 5 μL of SDS sample buffer (250 mM Tris, pH6.8, 4% SDS, 40% glycerol, 5% 2-mercaptoethanol, 0.05% bromophenol blue), and incubated for 5 min at 70°C. For evaluation of Moe phosphorylation, cells were lysed in 20 mM Tris buffer (pH 7.5) containing 1% Triton X-100, 0.1% SDS, 1% sodium deoxycholate, 150 mM NaCl, EDTA-free protease inhibitor, and phosphatase inhibitor cocktail (Sigma). Moe-Flag proteins were precipitated from cell lysates by anti-Flag M2 Affinity Agarose Gel (Sigma). Proteins were separated using electrophoresis on 12.5% polyacrylamide gels and transferred to a Clear-TransSP PVDF membrane (Wako). For immunoblotting, the following primary antibodies were used: rabbit anti-GM130 (1:1000, Abcam, ab30637), rabbit anti-NRV2.1 (1:2000, GeneTex, GTX124112), rabbit anti-GFP (1:2000, MBL, 598), goat anti-LMNA/C (1:500, Santa Cruz Biotech, sc6215), rabbit anti-Flag (anti-DDDDK-tag) (1:2000, MBL, PM020), mouse anti-Phospho-Threonine (42H4) (1:1000, Cell Signaling Technology, 9386), rabbit anti-SESB (1:20000), and rabbit anti-DESAT1 (1:1000). Rabbit polyclonal antibodies against SESB and DESAT1 were generated against a 17-residue contiguous segment (MGKDFDAVGFVKDFAAC) of SESB and an 18-residue contiguous segment (DQPKEEIEDAVITHKKSE) of DESAT1, respectively (Murakami et al., 2017). The PVDF membranes were probed with primary antibodies, and bound antibodies were detected with Horseradish peroxidase (HRP)-conjugated goat anti-rabbit immunoglobulin (IgG) (1:2000, Bethyl, A120-101P), HRP-conjugated goat anti-mouse IgG (1:2000, GE Healthcare, NA931) and HRP-conjugated rabbit anti-goat IgG (1:1000, Santa Cruz Biotech, sc-2768) using Super Signal West Pico (Thermo Fisher Scientific) and Ez-Capture MG (Atto).

Ro09-0198 cellular toxicity assay

Cells (2×10^5) in a 48-well plate were incubated for 1 h in 200 μL of Schneider's *Drosophila* medium containing 0.1% BSA and 0–2 μM Ro09-0198 at 25°C. To measure the proportion of living cells, 40 μL of CellTiter AQuousOne (PROMEGA) was added to each well and the cells were incubated for 3 h at 25°C. The absorbance at 490 nm was measured with a micro plate reader infinite F200 PRO (Tecan).

京都大学 KYOTO UNIVERSITY
A Self-archived copy in
Kyoto University Research Information Repository
https://repository.kulib.kyoto-u.ac.jp
京都大学学術情報リポジトリ KURENAI 紅 Kyoto University Research Information Repository

NBD-labeled phospholipid incorporation assay

1-palmitoyl-2-{6-[(7-nitro-2-1,3-benzoxadiazol-4-yl)amino]hexanoyl}-*sn*-glycero-3-phosphoethanolamine (NBD-PE), 1-palmitoyl-2-{6-[(7-nitro-2-1,3-benzoxadiazol-4-yl)amino]hexanoyl}-*sn*-glycero-3-phosphoserine (NBD-PS), and 1-palmitoyl-2-{6-[(7-nitro-2-1,3-benzoxadiazol-4-yl)amino]hexanoyl}-*sn*-glycero-3-phosphocholine (NBD-PC) were purchased from Avanti Polar Lipids. Cells were washed with and suspended in ice-cold Hank's Balanced Salt Solution (HBSS). Cell suspension (600 μL) was incubated for 1 h on ice to inhibit endocytosis and mixed with 600 μL of ice-cold HBSS containing 400 nM NBD-PE, NBD-PC, or NBD-PS. After a three min incubation on ice, cells were incubated at 15°C for 0, 2, 4, 6, and 8 min. Endocytic incorporation at the plasma membrane is suppressed in our experimental conditions (15°C for up to 8 min) (Figure S4H). Then, 150 μL aliquots of cell suspension were mixed with 300 μL of ice-cold HBSS containing 5 mg/mL BSA. The fluorescence intensity of each cell was analyzed with a Cytomics FC500 instrument (Beckman). NBD-labeled phospholipid transport analyses were performed at least three times and representative data are shown in Figures 3D, S4I, and S4J.

Analysis of actin cortex thickness

Analysis of actin cortex thickness was performed as previously reported (Clark et al., 2013). Briefly, optical sections of cells co-expressing CD8-mRuby2 and Lifeact-EGFP were obtained using a confocal microscope (LSM710, Zeiss) with a 63X objective lens. Segmented cell boundaries were acquired using adaptive active contours (snakes) software, and the fluorescence intensity on the line perpendicular to the contour were measured using ImageJ software. Signals derived from microvilli or cytoplasmic aggregates were removed. The position and intensity of peaks were determined by fitting with a Gaussian function using the five points adjacent to and including the peak. The distance between the peaks of the actin cortex and the plasma membrane (Δ) was calculated from each peak position.

To estimate the actin cortex thickness, the actin cortex structure was fitted with a simplified model of cortex geometry as previously reported (Clark et al., 2013). In this model, the actin distribution near the cell surface is approximated using following equations:

$$L_x = i_{in} + (i_c - i_{in})\theta_{-h/2}(x - X_c) + (i_{out} - i_c)\theta_{h/2}(x - X_c) \quad \text{(Equation 3)}$$

where

$$\theta_\mu(x) = \begin{cases} 0 \text{ for } x < \mu \\ 1 \text{ for } x \geq \mu \end{cases}. \quad \text{(Equation 4)}$$

In these equations, h, i_c, i_{in}, and i_{out} represent thickness of actin cortex, intensity of actin cortex, intracellular background, and extracellular background, respectively.

The effect of diffraction during imaging was eliminated by convolving the actin distribution using a Gaussian function with a mean of zero and standard deviation (σ);

$$\tilde{L_x} = i_{in} + (i_c - i_{in}) \int_{-\infty}^{x - X_c + h/2} G_\sigma(\tau)\, d\tau + (i_{out} - i_c) \int_{-\infty}^{x - X_c - h/2} G_\sigma(\tau)\, d\tau \quad \text{(Equation 5)}$$

where

$$G_\sigma(x) = \frac{1}{\sqrt{2\pi\sigma^2}}\, e^{-\frac{x^2}{2\sigma^2}}. \quad \text{(Equation 6)}$$

The previously reported values for the standard deviation of Lifeact-EGFP and CD8-mRuby2 were used (Clark et al., 2013). After convoluting with the values for standard deviation, the experimental data were fitted to Equation 5. The center of the cortex (Xc) was determined using OriginPro software (OriginLab).

Preparation of giant plasma membrane vesicles (GPMVs)

Kc167 cells (1×10^7 cells) were incubated in a six-well plate for 1 h at 37°C in GPMV buffer (10 mM HEPES, pH 7.4, 150 mM NaCl, 2 mM $CaCl_2$) containing 5 mM N-ethylmaleimide and 5 mM dithiothreitol (Sezgin et al., 2012) to induce the formation of GPMVs.

Flicker spectroscopy of GPMVs

GPMVs in GPMV buffer were mixed with equal volumes of hypertonic GPMV buffer (10 mM HEPES, pH 7.4, 190 mM NaCl, 2 mM $CaCl_2$). A phase contrast image of GPMVs was obtained using an Axiovert 200 optical microscope (Carl-Zeiss) at 25°C in glass bottom dishes (MetTek) coated with PBS containing 0.1% BSA. Flicker spectroscopy analyses were performed by using self-written codes on Igor Pro (Wave Metrics, Olegon), as previously reported (Brochard and Lennon, 1975). Briefly, the position of the GPMV rim was detected by taking the peak position of the intensity gradient profile along the radial direction and represented in a polar coordinate (R, θ), with the origin being the position of the center of mass at each frame ($0 \leq \theta < 2\pi$). The radial profile at each time point $R(\theta, t)$ was then normalized to obtain the fluctuation amplitude r (θ, t):

$$r(\theta, t) \equiv R(\theta, t) - \langle R(\theta, t) \rangle_\theta. \quad \text{(Equation 7)}$$

京都大学 KYOTO UNIVERSITY
A Self-archived copy in
Kyoto University Research Information Repository
https://repository.kulib.kyoto-u.ac.jp
京都大学学術情報リポジトリ KURENAI 紅 Kyoto University Research Information Repository

The angle brackets mean the average over the circumferential direction.

The fluctuation profiles were then Fourier-transformed into the mean square amplitude using Equation 8:

$$\left\langle u(q,t)^2 \right\rangle_t = \left\langle \frac{1}{N}\sum_{n=0}^{N-1}\left| r\left(\frac{2\pi n}{N},t\right)e^{-2\pi iqn/N}\right|^2 \right\rangle_t, \quad \text{(Equation 8)}$$

where N and q represent the sampling number (N = 256) and the wavenumber, respectively. Theoretically, this spectrum can be derived from the free energy of a thermally fluctuating lipid membrane by approximating the membrane–cytoskeleton coupling as a harmonic potential (Gov and Safran, 2005):

$$\left\langle u(q,t)^2 \right\rangle_t = \frac{k_B T}{L}\sqrt{\frac{\kappa}{2(\sigma^2-4\kappa\gamma)}}\left[\frac{1}{\sqrt{2\kappa q^2+\sigma-\sqrt{\sigma^2-4\kappa\gamma}}}-\frac{1}{\sqrt{2\kappa q^2+\sigma+\sqrt{\sigma^2-4\kappa\gamma}}}\right], \quad \text{(Equation 9)}$$

κ, σ, γ, and L represent the bending stiffness, membrane tension, effective "spring constant" for membrane–cytoskeleton coupling, and contour length ($2\pi R_\theta$), respectively. Three fitting parameters, κ, σ, and γ, were determined by yielding the best-fit of Equation 9 to the experimental spectrum of each GPMV calculated from Equation 8.

Cellular deformation analysis under microchannel flow

The microfluid (Figure 6A) was manufactured as previously reported (Tatsumi et al., 2015). Cells (1×10^7) were washed with PBS and suspended in PBS containing 8% polyvinylpyrrolidone K-90 (MW 3.6×10^5, Nacalai tesque). Cells were introduced into the microfluid at increasing flow rates (1.5–18 μL/min) using a micro-syringe pump. The shapes of cells passing through the 50-μm wide microchannel were observed using a high-speed video camera Phantom V7.3 (Vision Research). Width (x) and height (y) of cells were determined using ImageJ software. The Deformation Index was calculated using Equation 10.

$$\text{Deformation Index} = \frac{x-y}{x+y} \quad \text{(Equation 10)}$$

Fluorescence recovery after photobleaching assay

Fluorescence recovery after photobleaching (FRAP) assays were performed as previously reported (Fritzsche et al., 2014). Briefly, bleaching was performed with a 488-nm beam operating at 100% laser power over the desired region (2 μm x 2 μm) centered on the plasma membrane using an LSM800 confocal microscope (Carl-Zeiss). 10 frames of view were acquired for normalization of the fluorescence intensity (I_0), and recovery was monitored over 30 frames of view. Fluorescence intensity of a small rectangular region (0.77 μm × 1.54 μm) centered on the bleached regions of the plasma membrane (I_t) was monitored using ZEN software (Carl-Zeiss). The mobile fraction (A) was calculated from the experimental data by fitting to Equation 11, where τ represents recovery rate, using OriginPro software (OriginLab).

$$I_t / I_0 = A\left(1-e^{-\tau t}\right) \quad \text{(Equation 11)}$$

Isolation of circulating and resident hemocytes

Circulating and resident hemocytes were isolated from male wandering third instar larva of *Drosophila melanogaster* (Petraki et al., 2015). The larvae were washed with PBS and placed in 5–10 μL of Schneider's *Drosophila* Medium on the slide glass. The posterior and anterior ends of larvae were dissected with scissors and bled for 30 s without any physical agitation to avoid disturbing resident hemocytes. The larvae were then transferred to another medium drop on glass slides and scraped or jabbed with a sharp needle to dissociate the resident hemocytes from the larval body wall. The number of circulating and resident hemocytes was counted using an Axiovert 200M microscope (Carl-Zeiss) and ImageJ software.

Molecular dynamics simulations

Two model lipid bilayers, which corresponded to symmetrical and asymmetric insect membranes, were created with the compositions shown in Figure S6A. The composition of the asymmetric membrane was deduced from available experimental data. The symmetric membrane was built under the assumption that the scramblases equalize the content of phospholipids but do not act on ceramide lipids (Bhat et al., 2015), thus leaving their distribution unmodified. For the sake of simplicity, all lipid species are represented by a single set of fatty acid tails – either palmitoyl-oleoyl (for PE, PS and PI lipids) or di-palmitoyl (for PC and CerPE lipids). Each membrane model contained 7,200 lipids arranged into a square periodic box with sides of ~50 nm in the X and Y dimensions (Figure 5A). The MARTINI coarse-grained force field version 2.2 (Marrink et al., 2007) was used. The systems were solvated by ~600,000 polarizable coarse-grained water beads (Yesylevskyy et al., 2010). Total 756 coarse-grained sodium ions were added to neutralize the negative charge of the system. All simulations were performed in Gromacs 2018.2 (Hess et al., 2008; Páll et al., 2015) at a temperature of 320 K in NVT ensemble with recommended simulation parameters for the MARTINI force field (Marrink et al., 2007). The Pteros molecular modeling library (Yesylevskyy, 2015) was used for system preparation and analysis. To mimic the micropipette aspiration

京都大学 KYOTO UNIVERSITY
A Self-archived copy in
Kyoto University Research Information Repository
https://repository.kulib.kyoto-u.ac.jp
京都大学学術情報リポジトリ KURENAI 紅 Kyoto University Research Information Repository

assay, the following setup was used. A wall of dummy particles, which simulated the rigid wall of the micropipette, was added on top of the membrane (shown in green). The wall extended over the whole simulation box in the XY plane and had a circular hole in the center with a diameter of 30 nm, with an attached cylindrical tube in the Z dimension that mimicked the lumen of the micropipette. Each dummy particle of the wall extended from the anchor, which was fixed in space and did not interact with any other atoms in the system, and the shell particle, connected to the anchor by harmonic bond. Shell particles interact repulsively with the atoms of lipid tails (Lennard-Jones parameters C6 = 0, C12 = 0.001 in Gromacs units), which made the wall impermeable to lipids. The aspiration process was modeled as following. Another layer of dummy particles, referred to as the piston and spanning the whole simulation box in the XY plane, was added at an initial distance of ~13 nm below the membrane (shown in red). The piston particles interacted repulsively with water (Lennard-Jones parameters C6 = 0, C12 = 0.01 in Gromacs units) and divided the solvent into two disconnected parts – below and above the membrane. In the course of the simulation, the piston particles were restrained by harmonic potentials in the Z dimension with a force constant of 1000 $kJ \cdot nm^{-2}$ and the centers of these restraining potential were moving toward the membrane with constant velocity v. As a result, the piston created excess pressure under the membrane and negative pressure above the membrane. This pressure pushed the membrane toward the impermeable wall of the "pipette" and extruded it through the hole. The viscoelastic response of the membrane was monitored by measuring the reaction force F_r acting on each particle of the piston in the Z dimension. We assumed that $F_r = kV$, where V is the excess volume of water pumped by the piston and k was the effective rigidity coefficient. k was found by linear fitting of F_r as shown in Figures 5B–5D. We are aware that k defined in this manner is not directly comparable with any of the experimental elastic characteristics of the membrane; however, it provides a simple quantitative measure of membrane rigidity in simulations. Larger values of k result in more rigid and harder to deform membranes. Both membranes were equilibrated for 250 ns with fixed piston position. After that, three independent simulations were performed for each of the systems: with the piston velocity $v = 10^{-4}$ nm/ps for 40 ns, with $v = 10^{-5}$ nm/ps for 300 ns, and with $v = 10^{-6}$ nm/ps for 700 ns.

QUANTIFICATION AND STATISTICAL ANALYSIS

The statistical significance of differences between the mean values was analyzed using the un-paired two-tailed t test. Multiple comparisons were performed using Tukey's test following ANOVA. A P value < 0.05 was considered to be statistically significant. Please note that statistical details are found in the figure legends.

京都大学 KYOTO UNIVERSITY
A Self-archived copy in
Kyoto University Research Information Repository
https://repository.kulib.kyoto-u.ac.jp
京都大学学術情報リポジトリ KURENAI 紅 Kyoto University Research Information Repository

Cell Reports, Volume *35*

Supplemental information

Extreme deformability of insect cell membranes is governed by phospholipid scrambling

Akifumi Shiomi, Kohjiro Nagao, Nobuhiro Yokota, Masaki Tsuchiya, Utako Kato, Naoto Juni, Yuji Hara, Masayuki X. Mori, Yasuo Mori, Kumiko Ui-Tei, Motohide Murate, Toshihide Kobayashi, Yuri Nishino, Atsuo Miyazawa, Akihisa Yamamoto, Ryo Suzuki, Stefan Kaufmann, Motomu Tanaka, Kazuya Tatsumi, Kazuyoshi Nakabe, Hirofumi Shintaku, Semen Yesylevsky, Mikhail Bogdanov, and Masato Umeda

京都大学 KYOTO UNIVERSITY
A Self-archived copy in
Kyoto University Research Information Repository
https://repository.kulib.kyoto-u.ac.jp
京都大学学術情報リポジトリ KURENAI 紅 Kyoto University Research Information Repository

Table S1. Phospholipid composition in cultured cell lines. Related to **Figure 2**.

		PE	PC	PS	CerPE	PI	SM
Kc167	(n = 4)	59.1 ± 2.4	21.8 ± 3.2	6.6 ± 0.7	3.5 ± 0.3	9.0 ± 1.0	n.d.
XKR-deficient #122	(n = 4)	53.9 ± 1.1	23.8 ± 1.6	8.9 ± 0.9	4.3 ± 0.5	9.1 ± 1.2	n.d.
CDC50-deficient	(n = 3)	65.0 ± 0.3	15.2 ± 1.0	9.8 ± 0.9	2.1 ± 0.6	7.8 ± 0.8	n.d.
Kc167 PM	(n = 4)	65.1 ± 2.5	12.4 ± 3.3	11.2 ± 2.8	5.9 ± 1.7	5.3 ± 1.9	n.d.
S2	(n = 3)	54.2 ± 1.5	24.2 ± 0.8	8.2 ± 0.3	5.5 ± 1.5	7.9 ± 1.0	n.d.
GM2	(n = 3)	50.4 ± 1.7	24.8 ± 1.0	10.8 ± 1.5	5.5 ± 0.6	8.6 ± 0.3	n.d.
BG2-c2	(n = 3)	63.3 ± 0.8	21.9 ± 0.6	3.1 ± 0.2	4.9 ± 0.2	6.8 ± 0.4	n.d.
BG2-c6	(n = 3)	56.7 ± 1.0	22.9 ± 0.6	7.6 ± 0.5	4.3 ± 0.2	8.5 ± 0.5	n.d.
BG3-c2	(n = 3)	50.0 ± 1.9	28.1 ± 1.7	8.1 ± 0.4	6.1 ± 0.2	7.6 ± 0.2	n.d.
C6/36	(n = 4)	40.7 ± 3.1	26.4 ± 2.8	6.7 ± 0.8	10.7 ± 1.0	8.6 ± 2.7	6.9 ± 1.2
CHO-K1	(n = 3)	12.3 ± 0.0	59.3 ± 0.8	9.1 ± 1.1	n.d.	8.2 ± 1.2	11.1 ± 0.6
THP-1	(n = 3)	22.5 ± 2.5	57.2 ± 1.9	5.8 ± 0.7	n.d.	7.2 ± 0.6	7.3 ± 1.6

Phosphatidylethanolamine (PE), phosphatidylcholine (PC), phosphatidylserine (PS), phosphatidylinositol (PI), ceramide phosphoethanolamine (CerPE), and sphingomyelin (SM) were separated from the cellular total lipid extract by two-dimensional TLC using a first solvent system of chloroform/methanol/acetic acid (65:25:10, v/v/v) and a second solvent system of chloroform/methanol/formic acid (65:25:10, v/v/v) on a silica plate. The amounts of phospholipid were determined by inorganic phosphate quantification. PM, plasma membrane. Mean ± SD. n.d., not detected.

京都大学 KYOTO UNIVERSITY
A Self-archived copy in
Kyoto University Research Information Repository
https://repository.kulib.kyoto-u.ac.jp
京都大学学術情報リポジトリ KURENAI 紅 Kyoto University Research Information Repository

Table S2. Elastic parameters in the cultured cell lines. Related to **Figures 1, 2, 4, 5, 6, and 7.**

	Membrane tension (pN/μm)			Young's modulus (Pa)			n
Kc167	27.8	±	16.4	21.4	±	7.2	42
XKR-deficient #122	113	±	61.5	57.4	±	22.9	41
XKR-deficient #160	91.9	±	46.2	50.3	±	21.0	20
XKR-deficient #122 / XKR	32.6	±	17.1	20.6	±	7.4	42
XKR-deficient #122 / AaXKR	33.9	±	20.4	21.8	±	11.6	25
CDC50-deficient	22.8	±	12.7	17.8	±	5.1	42
S2	18.5	±	7.0	20.7	±	5.5	23
BG2-c6	21.5	±	8.6	16.9	±	6.4	23
C6/36	24.4	±	11.1	21.9	±	7.0	20
THP-1	219	±	122	71.5	±	27.6	31
CHO-K1	289	±	152	198	±	109	22
CHO-K1 / EGFP	304	±	87.5	212	±	71.9	20
CHO-K1 / mXkr8	310	±	61.4	190	±	39.7	20
CHO-K1 / AaXKR	201	±	87.6	126	±	49.4	24
CHO-K1 +CytoD	23.2	±	9.0	14.7	±	6.4	21
Kc167 +CytoD	10.0	±	6.5	8.7	±	5.0	26
XKR-deficient #122 +CytoD	29.3	±	19.2	16.4	±	9.9	19
Kc167 / Mock	35.3	±	7.9	15.6	±	3.0	13
Kc167 / Moe	25.7	±	8.6	15.0	±	2.8	20
Kc167 / MoeTA	28.9	±	8.4	21.2	±	3.9	21
Kc167 / MoeTD	69.6	±	24.0	35.1	±	7.5	21
XKR-deficient #122 / Mock	118	±	60.1	58.3	±	30.4	13
XKR-deficient #122 / Moe	92.6	±	43.2	45.4	±	13.5	20
XKR-deficient #122 / MoeTA	65.2	±	20.3	40.8	±	15.2	21
XKR-deficient #122 / MoeTD	105	±	30.4	55.3	±	22.8	23
He-Gal4>w^{1118}	27.7	±	7.8	19.3	±	3.7	22
He-Gal4>UAS-dsXKR#1	61.1	±	25.6	55.6	±	19.2	22
He-Gal4>UAS-dsXKR#2	69.1	±	24.2	47.5	±	10.1	21

The numerical values for the membrane tensions and Young's moduli shown in Figures 1D, 1E, 2D, 2E, 4B, 4C, 5G, 5H, 6D, 6E, 7A, and 7B. Mean ± SD.

京都大学 KYOTO UNIVERSITY
A Self-archived copy in
Kyoto University Research Information Repository
https://repository.kulib.kyoto-u.ac.jp
京都大学学術情報リポジトリ KURENAI 紅 Kyoto University Research Information Repository

Table S3. Cholesterol/phospholipids ratio in the cultured cell lines. Related to **Figure 2**.

	Cholesterol/Phospholipid (mol/mol)
Kc167	0.059± 0.003
XKR-deficient #122	0.058± 0.001
CHO-K1	0.342± 0.006

Cholesterol content was determined by enzyme assay using Cholesterol E-test wako. The amount of phospholipids were determined by inorganic phosphate quantification. Mean ± SD.

京都大学 KYOTO UNIVERSITY
A Self-archived copy in
Kyoto University Research Information Repository
https://repository.kulib.kyoto-u.ac.jp
京都大学学術情報リポジトリ KURENAI 紅 Kyoto University Research Information Repository

Table S4. Primer sequences for RNA interference of *Drosophila* cells. Related to **STAR Method** and **Figure S3**.

Gene		Sequence (5' to 3')
GFP	Forward	ATTAATACGACTCACTATAGGGAGGAGGGCGAGGAGCTGTTCACC
	Reverse	ATTAATACGACTCACTATAGGGAGGCTCGTCCATGCCGAGAGTG
CDC50	Forward	ATTAATACGACTCACTATAGGGAGGAGCTGATCATCGACTACACCAAGTGCAGGCGCT
	Reverse	ATTAATACGACTCACTATAGGGAGGGTGGAGAGTATCATTCGCTTCGTGCCGTCGAA
XKR	Forward	TAATACGACTCACTATAGGGAGGAAGTGGACGCCCTTATGATG
	Reverse	TAATACGACTCACTATAGGGAGAGGCGATGTGGCGGTAGTATGTG
TMEM16	Forward	TAATACGACTCACTATAGGGAGAGCTCATCCGGACACCCTTCG
	Reverse	TAATACGACTCACTATAGGGAGACGAGGGATTGTCAAAGAGAT
ATP8A	Forward	TAATACGACTCACTATAGGGAGAGAACTTCGTATCGCTTTCGCA
	Reverse	TAATACGACTCACTATAGGGAGACGACTTCAAGACCAAGAGCC
ATP8B	Forward	TAATACGACTCACTATAGGGAGAGCTGTCCACATCCGAGCCAA
	Reverse	TAATACGACTCACTATAGGGAGAACCACCACGCCATAGCACCA
ATP9	Forward	TAATACGACTCACTATAGGGAGAAAGCGAGGAGTCAGGAAACATGG
	Reverse	TAATACGACTCACTATAGGGAGACAGCTCCAGGAACTCTGGTC
ATP10	Forward	TAATACGACTCACTATAGGGAGATCCTAGTAATGGCCAAACGGA
	Reverse	TAATACGACTCACTATAGGGAGAGAGCTCCATTTGCTGGGTAAATAG
ATP11	Forward	TAATACGACTCACTATAGGGAGAACGGCGAACTTGGACGGA
	Reverse	TAATACGACTCACTATAGGGAGAGGCGACCAGGATGACAATCA
ATP11	Forward	TAATACGACTCACTATAGGGAGAGGTGTTGGCCTTACGGTAGA
	Reverse	TAATACGACTCACTATAGGGAGAAGACTCTGGAGTCGTCGGAA

京都大学 KYOTO UNIVERSITY
A Self-archived copy in
Kyoto University Research Information Repository
https://repository.kulib.kyoto-u.ac.jp
京都大学学術情報リポジトリ KURENAI 紅 Kyoto University Research Information Repository

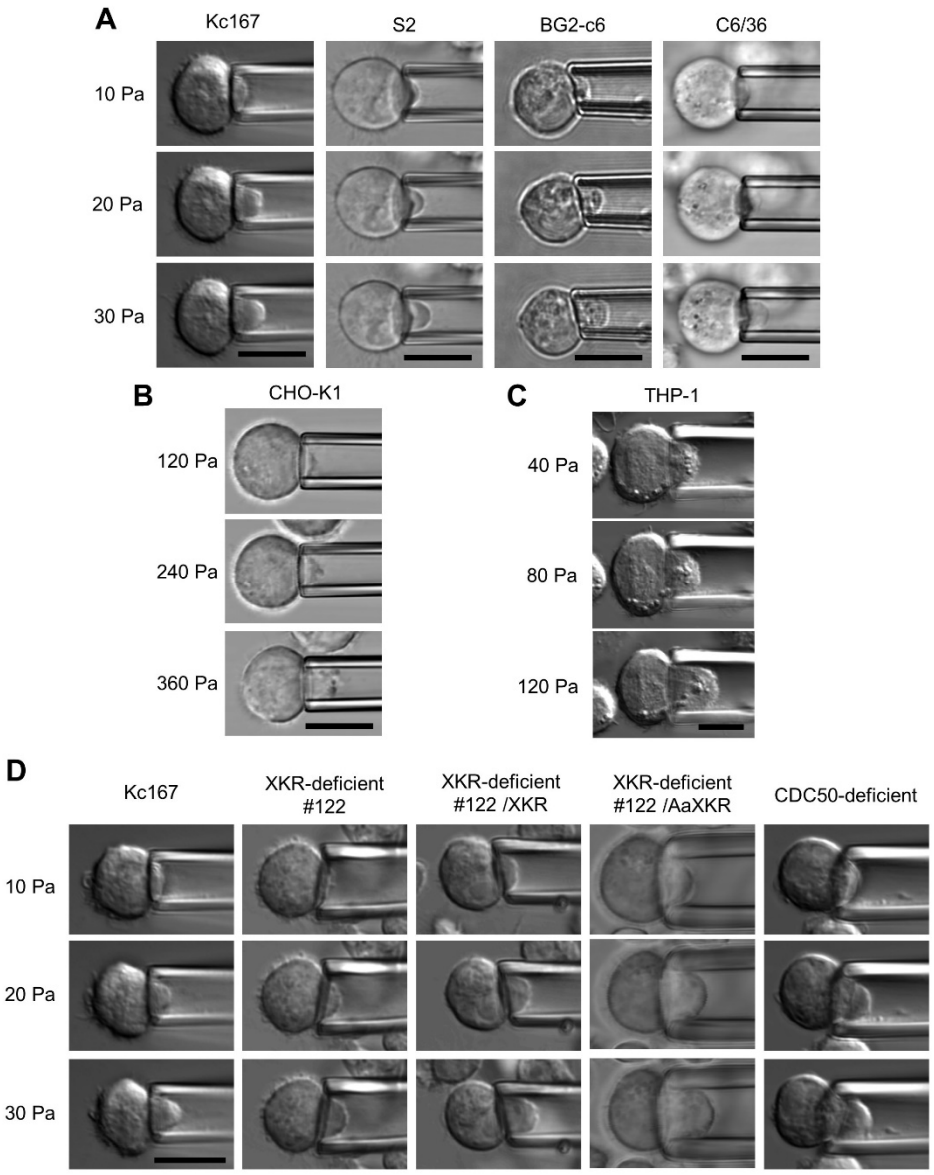

Figure S1. Measurement of elastic parameters in insect and mammalian cell lines. Related to **Figure 1** and **Figure 2**.

Insect cell lines (Kc167, S2, BG2-c6, C6/36, XKR-deficient #122, XKR-deficient #122 expressing XKR (XKR-deficient #122/XKR), and XKR-deficient #122 expressing AaXKR (XKR-deficient #122/AaXKR)) and mammalian cell lines (CHO-K1 and THP-1) were aspirated using cylindrical micropipettes at the indicated hydrostatic pressure. Scale bar, 10 μm.

京都大学 KYOTO UNIVERSITY
A Self-archived copy in
Kyoto University Research Information Repository
https://repository.kulib.kyoto-u.ac.jp
京都大学学術情報リポジトリ KURENAI 紅 Kyoto University Research Information Repository

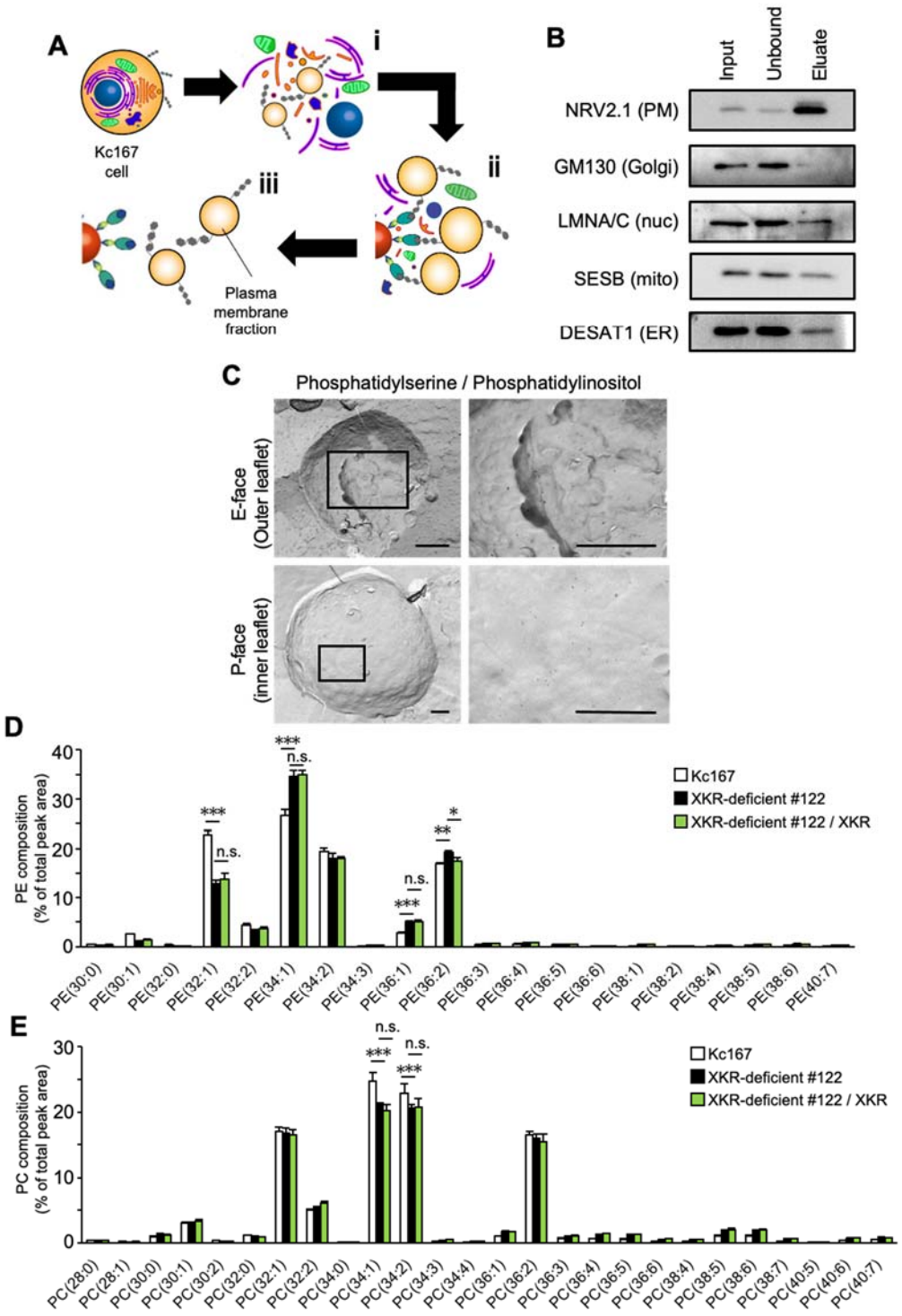

Figure S2. Analysis of composition and distribution of phospholipids in *Drosophila* cells. Related to **Figure 2**.

A, Experimental scheme for the isolation of plasma membrane fractions. (i) Kc167 cells were homogenized using glass beads. (ii) The plasma membrane fraction was bound to concanavalin A (ConA)-conjugated magnetic beads. (iii) The plasma membrane fraction was eluted from ConA-conjugated magnetic beads using methyl α-D-mannopyranoside. **B,** Homogenate (Input), unbound

京都大学 KYOTO UNIVERSITY
A Self-archived copy in
Kyoto University Research Information Repository
https://repository.kulib.kyoto-u.ac.jp
京都大学学術情報リポジトリ KURENAI 紅 Kyoto University Research Information Repository

fraction (Unbound), and purified plasma membrane fractions (Elute) were analyzed by immunoblotting. Anti-NRV2.1, anti-GM130, anti-LMNA/C, anti-SESB, and anti-DESAT1 antibodies were used as markers for the plasma membrane (PM), Golgi apparatus (Golgi), nucleus (nuc), mitochondria (mito), and endoplasmic reticulum (ER), respectively. **C,** Bound PS/PI-binding probes were labeled with gold-conjugated anti-mouse IgM antibody. Right panels are enlargement of the boxed area of left panels. Scale bar, 1 μm. **D, E,** PE (**D**) and PC (**E**) molecules in Kc167, XKR-deficient #122, and XKR-deficient #122 expressing XKR (XKR-deficient #122 / XKR) cells were analyzed by LC-MS/MS. Phospholipid molecules were presented in the format PE (X:Y) or PC (X:Y), where X denotes the total number of acyl chain carbons and Y denotes the total number of double bonds in acyl chains (n = 3). Values are expressed as Mean ± SD (**D, E**). * $P < 0.05$; ** $P < 0.01$; *** $P < 0.001$; n.s., not significant.

京都大学 KYOTO UNIVERSITY
A Self-archived copy in
Kyoto University Research Information Repository
https://repository.kulib.kyoto-u.ac.jp
京都大学学術情報リポジトリ KURENAI 紅 Kyoto University Research Information Repository

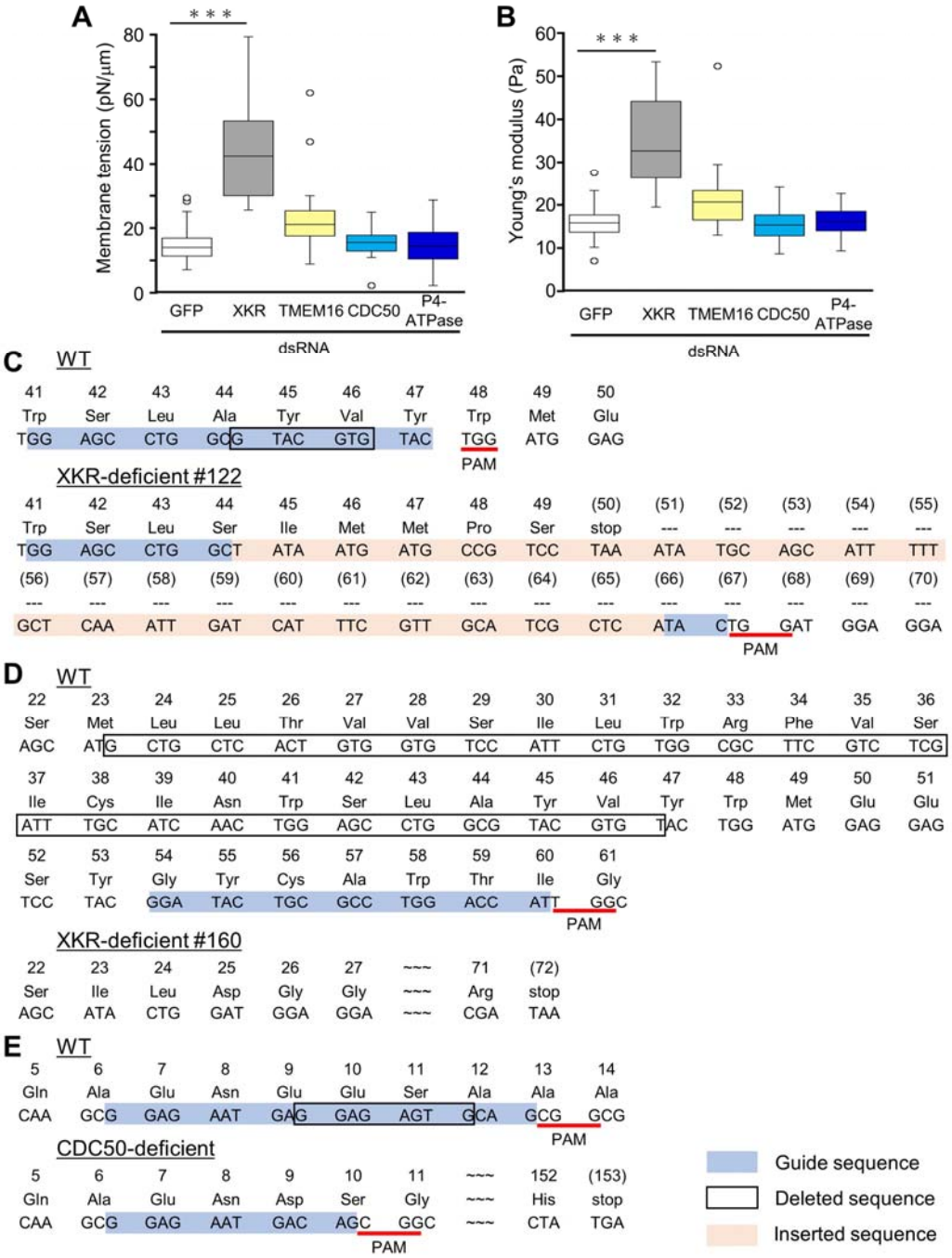

Figure S3. Contribution of phospholipid transporters to the regulation of deformability of *Drosophila* cell membranes. Related to **Figure 2**.

A, B, Membrane tensions and Young's moduli of Kc167 cells treated with dsRNA against *Gfp* (n = 23), *Xkr* (n = 20), *TMEM16* (n = 19), *Cdc50* (n = 21), or *P4-ATPases* (n = 20). For box plots, center mark is median, whiskers are minimum/maximum excluding outliers, and circles are outliers (**A, B**). Tukey's t-test (**A, B**). *** $P < 0.001$. **C-E,** Disruption of *Xkr* (**C, D**), and *Cdc50* (**E**) genes using CRISPR/Cas9 gene editing. The guide sequence and the protospacer-adjacent motif (PAM) are highlighted in blue and underlined in red, respectively. Deleted and inserted sequences are enclosed in boxes and highlighted in beige, respectively.

京都大学 KYOTO UNIVERSITY
A Self-archived copy in
Kyoto University Research Information Repository
https://repository.kulib.kyoto-u.ac.jp
京都大学学術情報リポジトリ KURENAI 紅 Kyoto University Research Information Repository

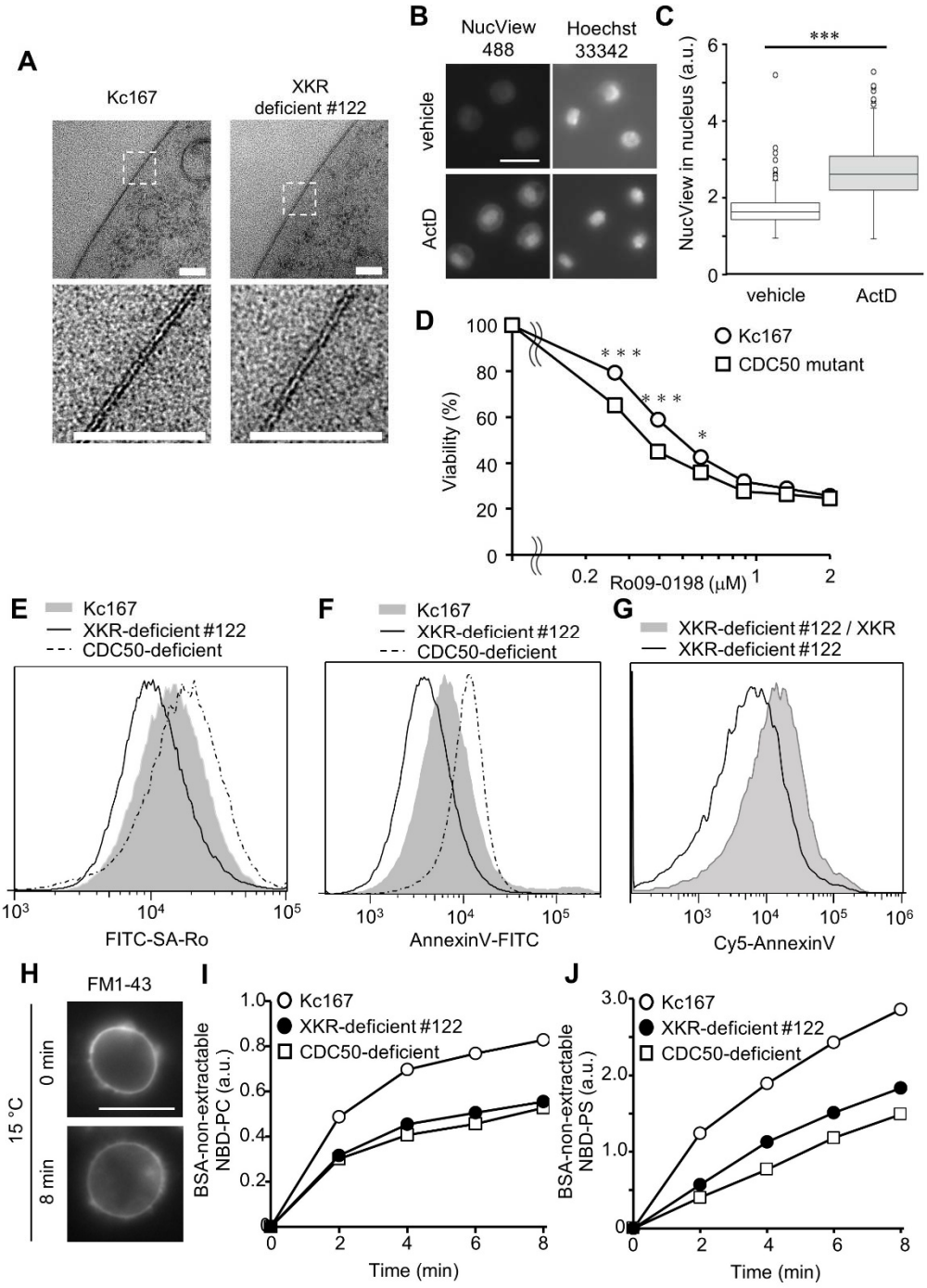

Figure S4. Effects of XKR depletion on the bilayer structure and phospholipid transport activities in the plasma membrane of *Drosophila* cells. Related to **Figure 3**.

A, (*top*) The plasma membranes of Kc167 and XKR-deficient #122 cells were observed using transmission electron microscopy. (*bottom*) Enlargement of the boxed area. Scale bar, 100 nm. **B,** Kc167 cells were incubated with actinomycin D (ActD) and NucView 488 for 6 h and fixed with 4% paraformaldehyde. The nuclei of apoptotic cells were stained with NucView cleaved by caspase. Scale bar, 10 μm. **C,** Fluorescence intensity of NucView in Kc167 cells treated with vehicle (n = 219) or ActD (n = 232). Apoptosis was effectively induced by ActD in Kc167 cells. **D,** Kc167 and CDC50-

京都大学 KYOTO UNIVERSITY
A Self-archived copy in
Kyoto University Research Information Repository
https://repository.kulib.kyoto-u.ac.jp
京都大学学術情報リポジトリ KURENAI 紅 Kyoto University Research Information Repository

deficient cells were incubated with Ro09-0198 in Schneider's *Drosophila* medium at 25°C for 1 h. Cellular viability was analyzed by MTS assay (n = 3). **E, F, G**, Staining of Kc167, XKR-deficient, CDC50-deficient, and XKR-deficient cells expressing XKR (XKR-deficient #122/ XKR) cells with FITC-SA-Ro (**E**), AnnexinV-FITC (**F**), or Cy5-AnnexinV (**G**). Dead cells stained with propidium iodide (PI) were excluded from analysis. Representative fluorescence activated cell sorting (FACS) profiles are shown. **H**, Kc167 cells were stained with FM1-43 dye on ice and incubated at 15°C for 8 min. Endocytosis of plasma membrane was suppressed under these experimental conditions. **I, J,** Trans-bilayer movement of NBD-PC (**I**) and NBD-PS (**J**) from the outer to inner leaflets of plasma membranes in Kc167, XKR-deficient #122, and CDC50-deficient cells. Cells were incubated with 0.4 μM NBD-PC or NBD-PS at 15°C for 0, 2, 4, 6, and 8 min. After washing with bovine serum albumin (BSA), fluorescence intensity was determined using flow cytometry. The mean fluorescence intensity of 20,000 cells (**I**) or 10,000 cell (**J**) at each incubation time is plotted. For box plots, center mark is median, whiskers are minimum/maximum excluding outliers, and circles are outliers (**C**). Student's t-test (**C, D**). *$P < 0.05$; *** $P < 0.001$.

京都大学 KYOTO UNIVERSITY
A Self-archived copy in
Kyoto University Research Information Repository
https://repository.kulib.kyoto-u.ac.jp
京都大学学術情報リポジトリ KURENAI 紅 Kyoto University Research Information Repository

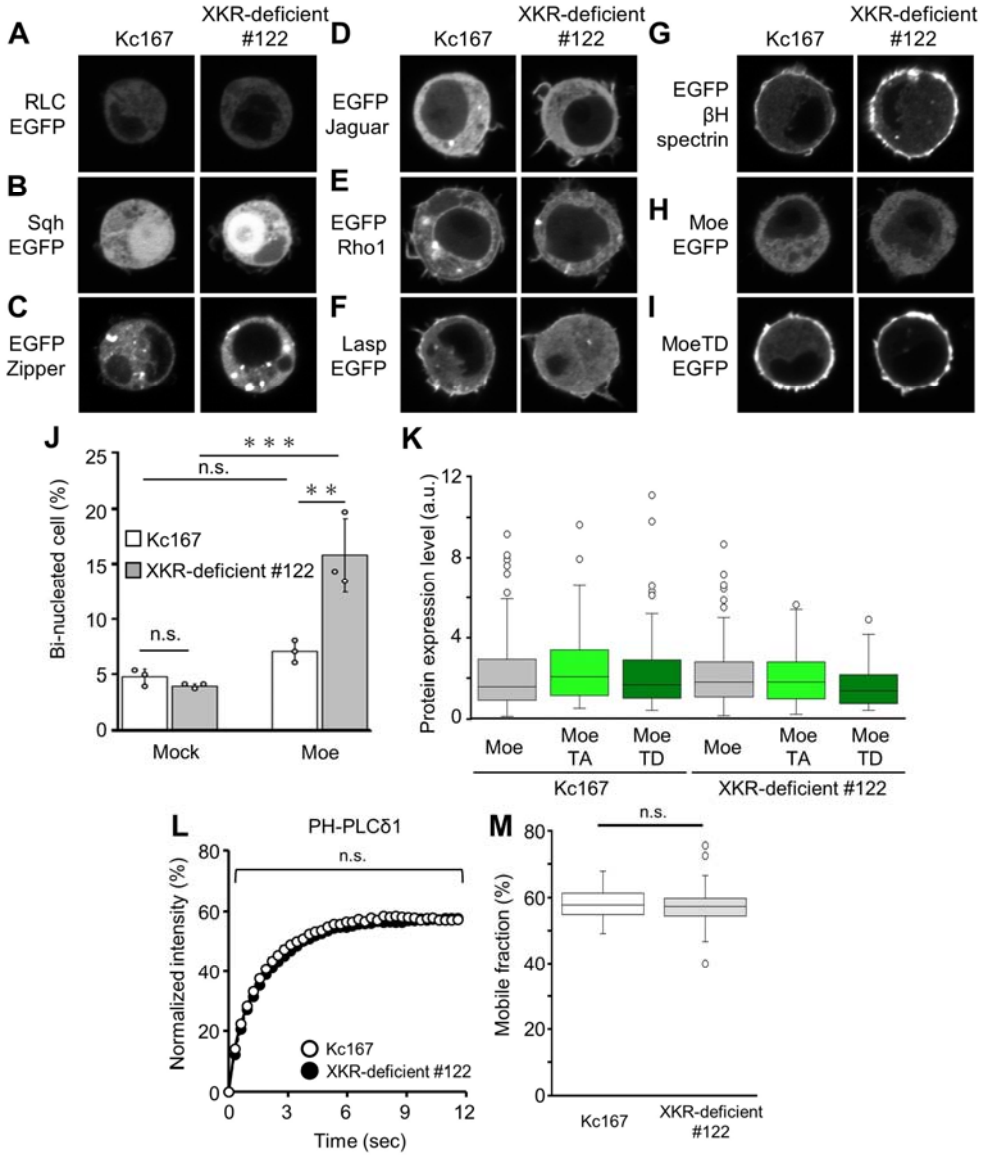

Figure S5. Effect of XKR depletion on the cytoskeleton proteins and phosphoinositide. Related to **Figure 4**.

A-I, Localization of RLC-EGFP (**A**), Sqh-EGFP (**B**), EGFP-Zipper (**C**), EGFP-Jaguar (**D**), EGFP-Rho1 (**E**), Lasp-EGFP (**F**), EGFP-βH-spectrin (**G**), Moe-EGFP (**H**), and MoeTD-EGFP (**I**) in Kc167 and XKR-deficient cells. Scale bar, 10 μm. **J**, Proportion of bi-nucleated cells in Kc167 and XKR-deficient cells expressing mock or Moe-EGFP. **K**, Protein expression levels of Moe-EGFP, MoeTA-EGFP, and MoeTD-EGFP in Kc167 and XKR-deficient cells. **L, M,** Normalized fluorescence recovery (**L**) and proportions of mobile fraction (**M**) in PH-PLCδ1-mClover on the plasma membrane of Kc167 (n = 39) and XKR-deficient cells (n = 42). For box plots, center mark is median, whiskers are minimum/maximum excluding outliers, and circles are outliers (**K**, **M**). Mean ± s.e.m. (**L**). Student's t-test (**L, M**). Tukey's test (**J, K**). ** $P < 0.01$;*** $P < 0.001$; n.s., not significant.

京都大学 KYOTO UNIVERSITY
A Self-archived copy in
Kyoto University Research Information Repository
https://repository.kulib.kyoto-u.ac.jp
京都大学学術情報リポジトリ KURENAI 紅 Kyoto University Research Information Repository

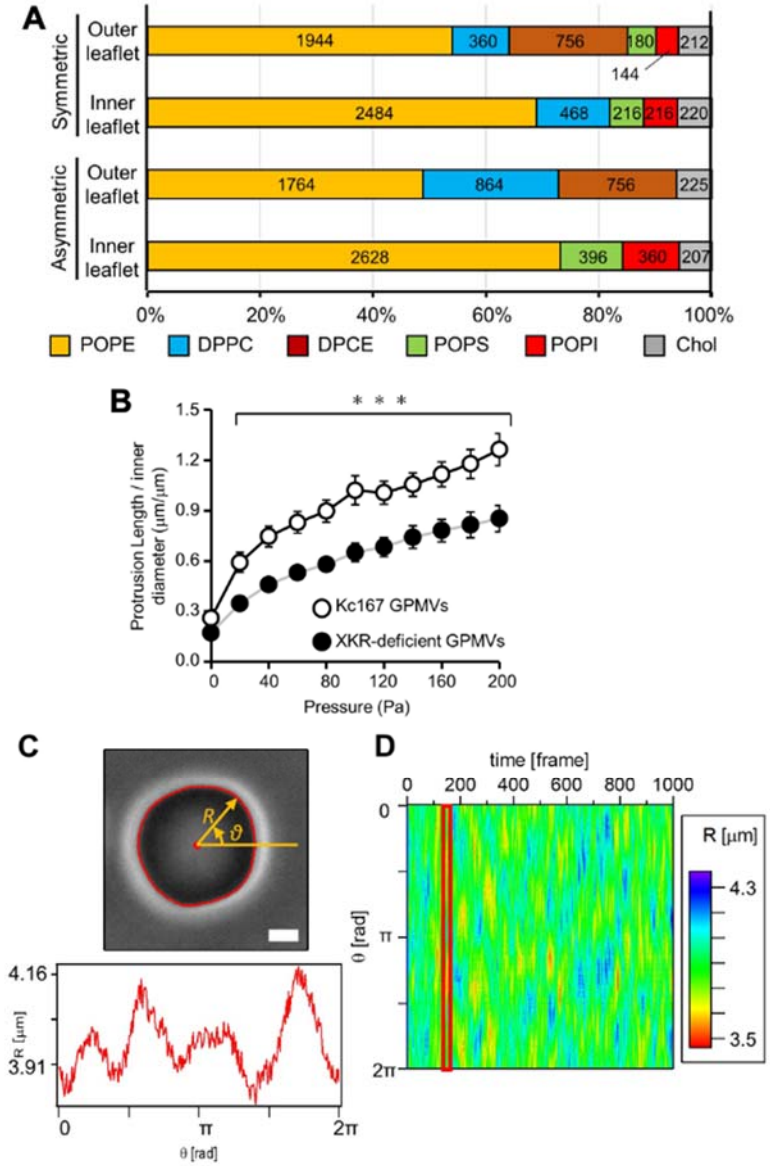

Figure S6. Role of XKR in the regulation of bilayer membrane deformability. Related to **Figure 5**.

A, The number of lipid molecules in each leaflet of bilayer membranes used in molecular dynamics simulations. POPE, 1-palmitoyl-2-oleoyl-sn-glycero-3-phosphoethanolamine; DPPC, 1,2-dipalmitoyl-sn-glycero-3-phosphocholine; DPCE, N-palmitoyl-D-erythro-sphingosylphosphoryl-ethanolamine; POPS, 1-palmitoyl-2-oleoyl-sn-glycero-3-phospho-L-serine; POPI, 1-palmitoyl-2-oleoyl-sn-glycero-3-phosphoinositol; Chol, cholesterol. **B,** GPMVs were aspirated using cylindrical micropipettes. Normalized protrusion length of GPMVs isolated from Kc167 (n = 15) and XKR-deficient (n = 13) cells were plotted. **C,** The position of the GPMV rim was detected by the intensity gradient profile along the radial direction (red), and represented in a polar coordinate (R, θ), with the origin being the position of the center of mass at each frame ($0 \leq \theta < 2\pi$). Scale bar, 2 μm. **D,** The radial profile at each time point R (θ, t) was represented in heat map. Mean ± s.e.m. (**B**). Student's t-test (**B**). *** $P < 0.001$.

京都大学 KYOTO UNIVERSITY
A Self-archived copy in
Kyoto University Research Information Repository
https://repository.kulib.kyoto-u.ac.jp
京都大学学術情報リポジトリ KURENAI 紅 Kyoto University Research Information Repository

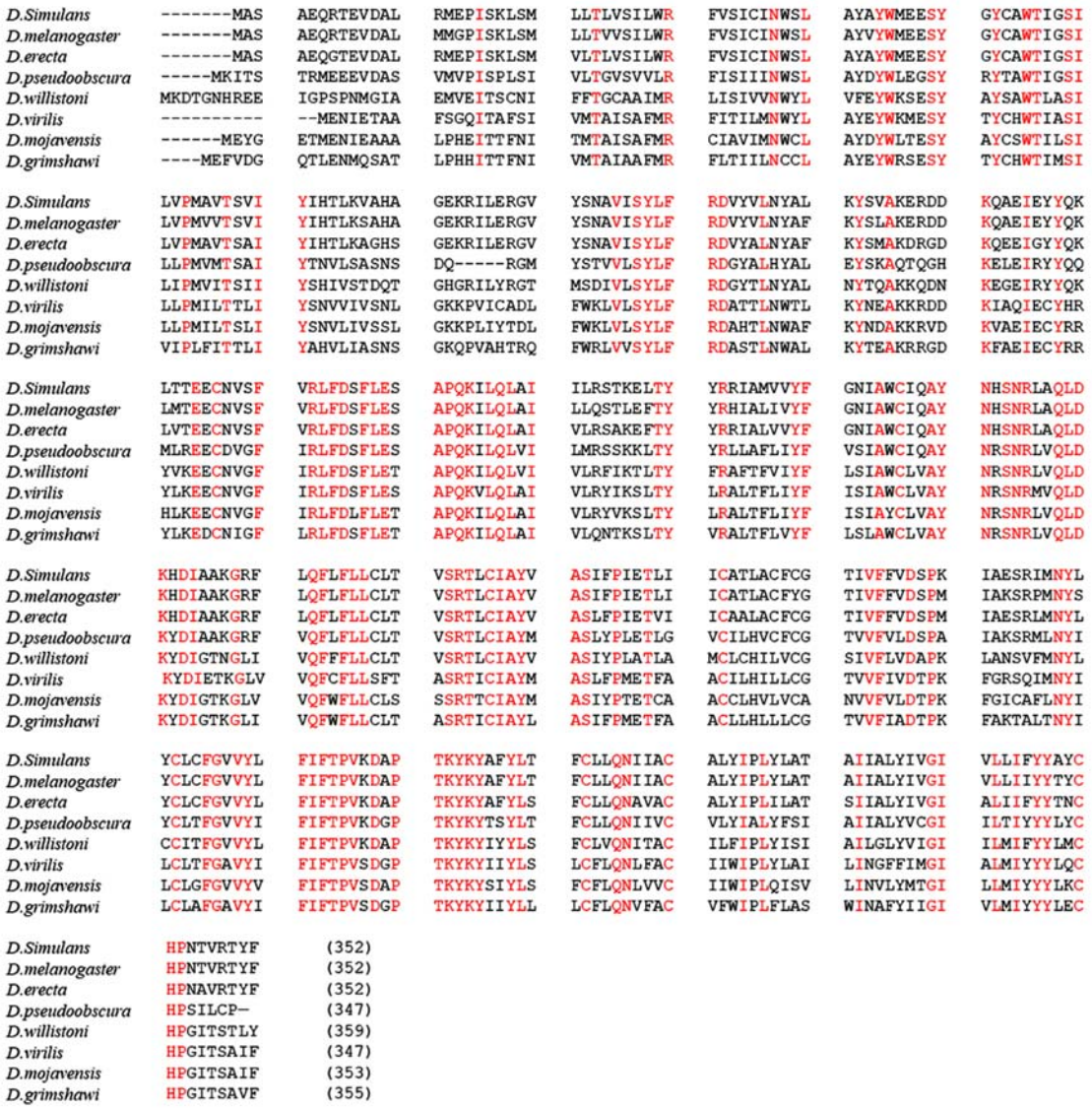

Figure S7. Amino acid sequences of *Drosophila* XKR proteins. Related to **Figure 3** and **Figure 7**. The amino acid sequences of XKR from eight *Drosophila* species were compared. *Drosophila simulans* (GD17275; EDX18076); *Drosophila melanogaster* (CG32579; NP_727957); *Drosophila erecta* (GG17953; EDV46885); *Drosophila pseudoobscura* (GA23155; XP_002134395); *Drosophila willistoni* (GK25056; EDW82581); *Drosophila virilis* (GJ19443; EDW65792); *Drosophila mojavensis* (GI10978; EDW05639); *Drosophila grimshawi* (GH12280; EDV99680). Conserved residues are shown in red.